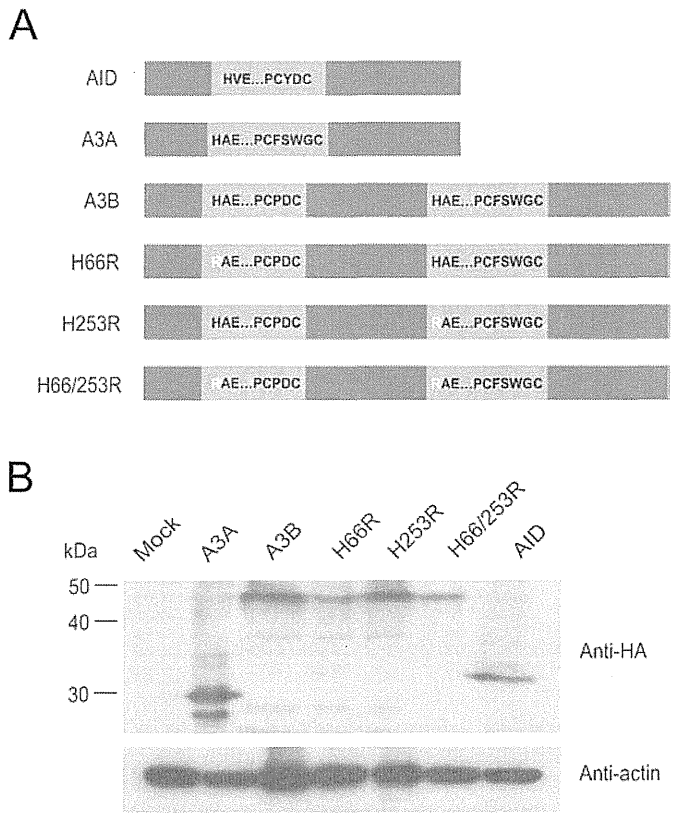

Figure 1 | Expression of A3A, A3B wild-type and mutants, and AID. (A) Schematic of expression vectors. The consensus amino acid residues for zinc-coordinating motifs are shown. Substituted residues are shown in white. (B) Expression of HA-tagged proteins. Expression vectors were transfected into HEK293 cells, and cell lysates were analyzed by immunoblotting with anti-HA antibody (top panel) and anti-ß-actin antibody (bottom panel) for loading control.

However, it is still unclear whether A3 proteins can induce somatic mutations into human genome with intact DNA repair systems. Here we first demonstrate that expression of A3B and A3A as well as AID can induce somatic mutations in genomic DNA in human cells even in the presence of UNG. We also find that high expression of A3B leads to somatic mutations in tumor-related genes. These data suggest that aberrant expression of A3B might be one of the active mechanisms that induce somatic mutations in cancer cells.

Results

A3 and AID induce hypermutations into foreign DNA. Besides A3A, we focused on A3B because it is localized predominantly in the nucleus[20,21] and highly expressed in many types of cancer cells[14] referring to microarray database (e.g., NextBio: http://www.nextbio.com). Previous studies have shown that A3B contains two enzymatically active CDAs in restricting HIV-1[22], whereas only carboxyl-terminal CDA is responsible for inhibiting HBV replication[23,24] and editing bacterial DNA[22]. A3B is also shown to restrict foreign DNA in mammalian cells[25], but it has not been tested which CDA is active in this context. First, to examine whether A3 and AID induce mutations in foreign DNA in human cells and which CDA is responsible for this DNA editing, we constructed amino- and/or carboxyl-terminal CDA mutants (H66R, H253R, and H66/253R) by site directed mutagenesis (Fig. 1a) and confirmed their expression in HEK293 cells by immunoblotting (Fig 1b). We transfected expression vectors for these together with EGFP expression vector into HEK293 cells and examined base substitutions in *EGFP* sequences. The expression vector for UNG inhibitor (UGI) was also co-transfected to avoid UNG-triggered degradation of uracil-containing foreign DNA as described previously[25]. We recovered total DNA from the cells 2 days after transfection and performed differential DNA denaturation PCR (3D-PCR) to efficiently recover edited DNA sequences[26]. 3D-PCR is based on the principle that DNA sequences with fewer interstrand hydrogen bonds dissociates easier. If cytidine deamination takes place frequently, resulting AT-rich *EGFP* gene can be amplified at lower denaturation temperatures. Although PCR products were obtained from all samples at 92°C of denaturation temperature (Td), we obtained robust PCR products at 83.8°C of Td only from A3A-, A3B wild-type (WT)-, and AID-expressing cells (Fig 2a). Amplification of *EGFP* at the lowest Td was impaired in H66R-expressing cells compared to A3B WT-expressing cells and undetectable in H253R- or H66/253R-expressing cells (Fig 2a, bottom). To ascertain whether *EGFP* gene was actually hyperedited, we cloned and sequenced the amplicons at 83.8°C of Td. As can be seen from the mutation matrices, high levels of C/G to T/A transitions were introduced into *EGFP* sequences (Fig 2b). To compare the extent of baseline mutations and that of A3B-induced mutations, we also cloned and sequenced the amplicons at 94.0°C of Td. Mutation frequency of A3B-expressing cells were about 6 times higher than that of mock-transfected cells (Supplementary Fig. S1 online). The mutation frequency in H66R-expressing cells was approximately a half compared to that in A3B WT-expressing cells in the amplicons at the lowest Td (Fig 2c). These data suggest that carboxyl-terminal CDA of A3B is mainly responsible for foreign DNA editing, but both domains are requisite for full editing activity. It is worth noting that AID is also capable of inducing cytidine deamination into foreign DNA.

Human A3 proteins have preferred target dinucleotide sequences in the substrate DNA; A3A and A3B prefer to deaminate cytosine residues flanked by 5′ thymine residue, 5′-TC, whereas A3G prefers to deaminate cytosine residues flanked by 5′ cytosine residue, 5′-CC[25,27–29]. We analyzed the context of C/G to T/A transitions in hyperedited *EGFP* sequences. We observed a strong bias toward deamination at 5′-TC dinucleotides in A3A-, A3B WT-, and H66R-expressing cells, but not in AID-expressing cells (Fig 2d). 5′-TC dinucleotide preference of A3B was also confirmed by sequencing amplicon at 94.0°C of Td which is supposed to be unbiased (Supplementary Fig. S1 online). These data suggest that the preference of editing sites in foreign DNA by A3s coincides with that seen in viral DNA.

A3A and A3B can edit genomic DNA in human cells. We next investigated whether A3 proteins induce C/G to T/A transitions into not only foreign DNA but also nuclear DNA in human cells. We first established a HEK293 cell line stably expressing EGFP (HEK293/EGFP) using retrovirus vector that carries *EGFP*. We transfected HEK293/EGFP cells with expression vectors for A3A, A3B WT or mutant (H66R, H253R, or H66/253R), or AID by lipofection, and then recovered total DNA from these cells after 7-day culture. We performed 3D-PCR of *EGFP* gene and obtained amplicons from A3A-, A3B WT-, H66R-, and AID-expressing cells at lower Td (Fig 3a). *EGFP* gene was recovered at Td as low as 86.3°C from A3B WT-expressing cells, while as low as 86.5°C from A3A-, H66R-, and AID-expressing cells. By contrast, *EGFP* gene was not amplified below Td of 87°C from cells transfected with mock, H253R or H66/253R. We repeated this procedure consisting of transfection, DNA extraction, and 3D-PCR three times and obtained similar results (Fig 3b). To unambiguously confirm the presence of C/G to T/A transitions, we cloned and sequenced amplicons obtained at the lowest Td in A3A-, A3B WT-, H66R-, and AID-expressing cells (Fig 3c). These analyses revealed approximately 2 to 5 C/G to T/A transitions per *EGFP* sequence from each sample (Fig 3d). The transitions were detected most frequently in A3A-expressing cells, and deaminase activity of H66R mutant was approximately a half

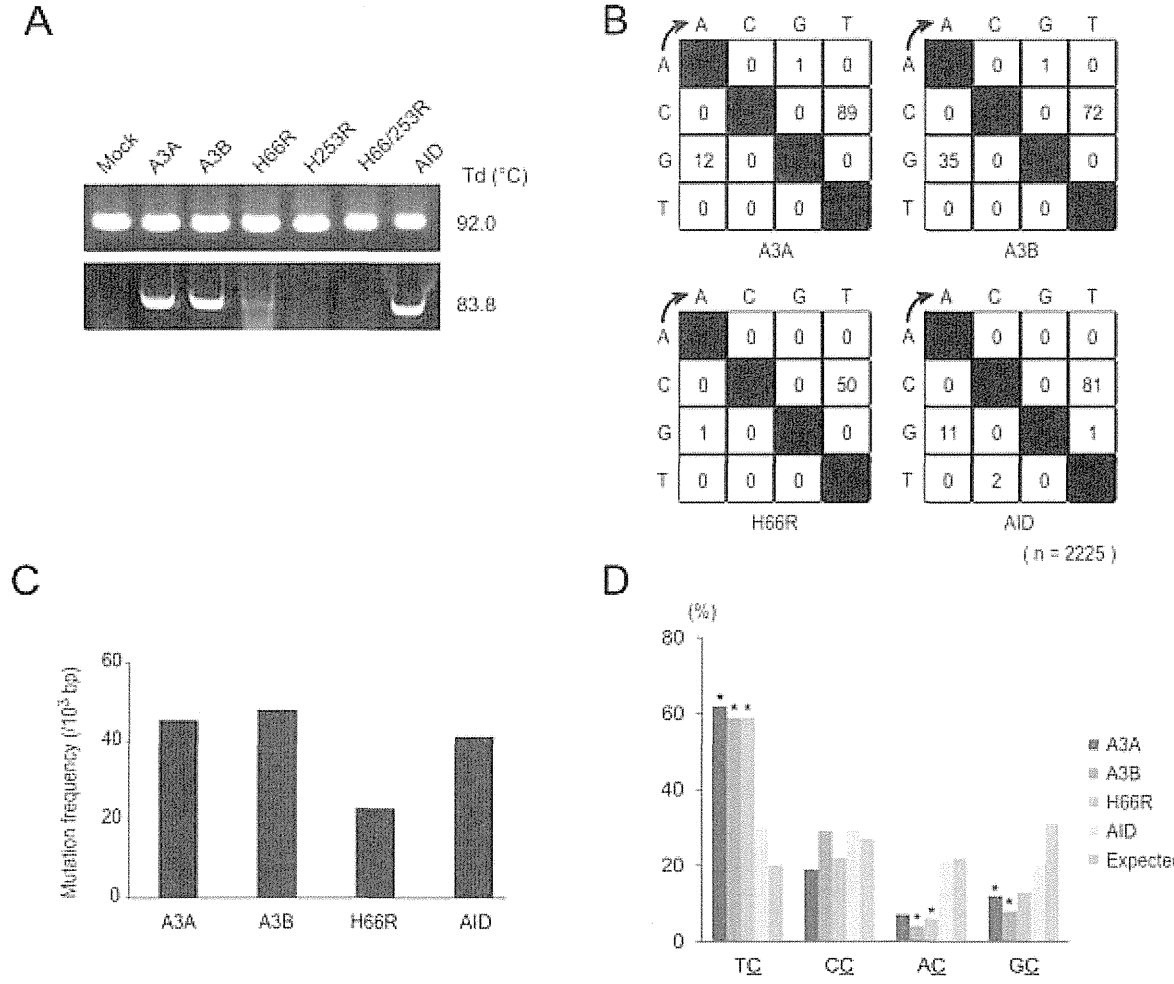

Figure 2 | Foreign DNA editing by A3A, A3B, and AID. (A) Agarose gel analyses of 3D-PCR products from HEK293 cells. Cells were transfected with expression vector for A3A, A3B wild-type or mutant, or AID together with pEGFP-N3 and pEF-UGI. Total DNA was recovered 2 days after transfection, and *EGFP* gene was amplified by 3D-PCR at the indicated denaturation temperatures (Td). (B) Mutation matrices of hyperedited *EGFP* sequences derived from cloned amplicons at 83.8°C of Td. "n" indicates the number of bases sequenced. We sequenced 5 clones (2,225 base pairs in total) in each group. (C) Frequencies of C/G to T/A transitions in hyperedited *EGFP* genes. C/G to T/A transitions per 1,000 sequenced base pairs are shown. (D) Dinucleotide contexts in foreign DNA editing. The rates of indicated dinucleotide sequence at the C to T transitions are shown. Asterisks indicate statistical significance in a χ^2 test ($p < 0.01$).

compared to that of A3B WT as seen in foreign DNA assays. The contexts of C/G to T/A transitions detected from the lowest Td amplicons in genomic DNA editing in A3-expressing cells were distinct from those in foreign DNA editing (Fig 3e). A preference for 5′-TC dinucleotide was not apparently observed, alternatively, 5′-GC dinucleotides were preferred in all samples. However, this bias fails to reach statistical significance ($p < 0.01$) in a χ^2 test. The preferred target sequences of AID editing were 5′-GC and 5′-AC dinucleotides as described by many prior studies[27,30]. Mutation frequencies and preferred target sequence of A3B was also analyzed by using amplicons at 94.0°C of Td. Mutation frequency of A3B-expressing cells were about 3 times higher than that of mock-transfected cells (Supplementary Fig. S2 online). A preference for 5′-TC dinucleotide was impaired, compared to that in foreign DNA editing assays (Supplementary Fig. S2 online). Our results reveal that in addition to AID, A3A and A3B can induce C/G to T/A transitions into human nuclear DNA without repressing proofreading enzymes (e.g., UNG). Mutation frequencies were 6 to 9 per 1000 base pairs in A3A-, A3B WT-, and AID-expressing cells, and much less frequent compared to those in foreign DNA editing. As seen with foreign DNA editing, carboxyl-terminal CDA is mainly responsible for catalytic activity but not sufficient for full editing activity. The preference context of genomic DNA editing by A3A and A3B is different from that of viral or foreign DNA editing.

Deep sequencing reveals hyperediting of human genomic DNA by A3 proteins. Amplicon sequencing by next-generation sequencer has enabled to detect extremely low levels of mutations of targeted regions in genomic DNA. To verify more certainly that A3 proteins edit human nuclear DNA, we performed deep sequencing of A3-expressing cells. HEK293/EGFP cells were transfected with an empty vector or expression vectors for A3A, A3B WT, H66/253R, or AID by lipofection, and total DNA were extracted after 7-day culture. We amplified a portion of *EGFP* gene with 443 base pair length (from thymine 56 to cytosine 498) by conventional PCR protocol, not by 3D-PCR, and performed amplicon sequencing with the coverage of 1337 to 2654 reads per sample. This analysis revealed that extremely large numbers of nucleotides were substituted over the full length of amplicons in A3A-, A3B WT-, and AID-expressing cells, whereas very few mutations were detected in mock and H66/253R-expressing cells (Supplementary Table 1 online). C/G to T/A transitions were observed most frequently in A3A-expressing cells as variation rates reach approximately 7% at the maximum, while below 3% at most in A3B- and AID-expressing cells (Fig 4a

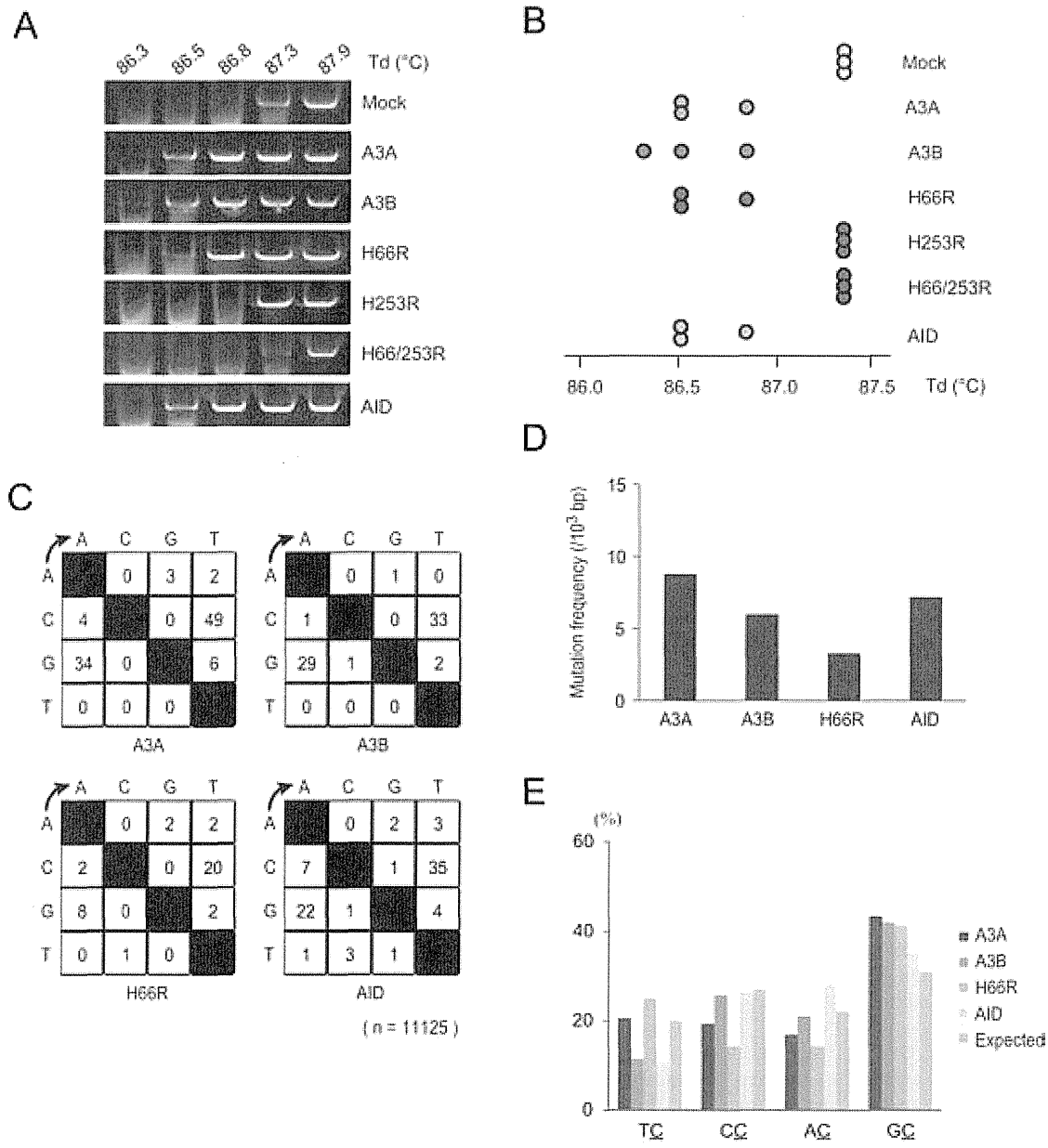

Figure 3 | Hypermutations in *EGFP* genes integrated in genomic DNA of HEK293 cells. (A) Agarose gel analyses of 3D-PCR products of *EGFP* genes extracted from HEK293/EGFP cells. Cells were transfected with expression vector for A3A, A3B wild-type or mutant, or AID. Total DNA was recovered 7 days after transfection and *EGFP* genes were amplified by 3D-PCR at the indicated denaturation temperatures (Td). (B) Distributions of the lowest denaturation temperatures for positive PCR amplification in each sample. Each circle represents independent experiment consisting of transfection, DNA extraction, and 3D-PCR. (C) Mutation matrices of hyperedited *EGFP* sequences derived from cloned PCR products at Td lower than 87°C. "n" indicates the number of bases sequenced. We sequenced 25 clones (11,125 base pairs in total) in each group. (D) Frequencies of C/G to T/A transitions in hyperedited *EGFP* genes. C/G to T/A transitions per 1,000 sequenced base pairs are shown. (E) Dinucleotide contexts in genomic DNA editing. The rates of indicated dinucleotide sequence at the C to T transitions are shown. Deviations in the editing contexts do not reach statistical significance ($p < 0.01$) in a χ^2 test.

and Supplementary Table 1 online). The mutation frequency analysis revealed that large numbers of C/G to T/A substitutions were induced in A3A-, A3B-, and AID-expressing cells, whereas other types of base substitutions were very few (Fig 4b). These results are similar to the data obtained by 3D-PCR and clonal sequencing of A3- and AID-expressing cells, and further demonstrated that A3A and A3B as well as AID can induce C/G to T/A transitions into genomic DNA in human cells with intact DNA repair systems. Dinucleotide preference of target sequence for deamination by A3A, A3B and AID was also analyzed, however, we did not found any preference in this experiment (Fig. 4C), suggesting the difference between foreign DNA editing and genomic DNA editing.

Expression of A3B and somatic mutations in lymphoma cells. Although AID has been reported to play important roles in lymphomagenesis by inducing mutations in both Ig and non-Ig genes[11,12,31–34], AID-independent mechanisms are also suggested, because AID is not expressed in all types of B-cell lymphomas[31,35]. We hypothesized that A3 may contribute to somatic mutations in some lymphoma cells. To examine this hypothesis, we first determined expression levels of *A3A*, *A3B*, and *AID* by quantitative RT-PCR in several B-cell lymphoma cell lines using peripheral blood lymphocytes (PBL) as control (Fig 5a). Our analysis revealed that *A3B* was highly expressed in 3 of 4 cell lines, particularly, markedly high in KIS1 cells, whereas expression of *A3A* transcripts was not detected in any

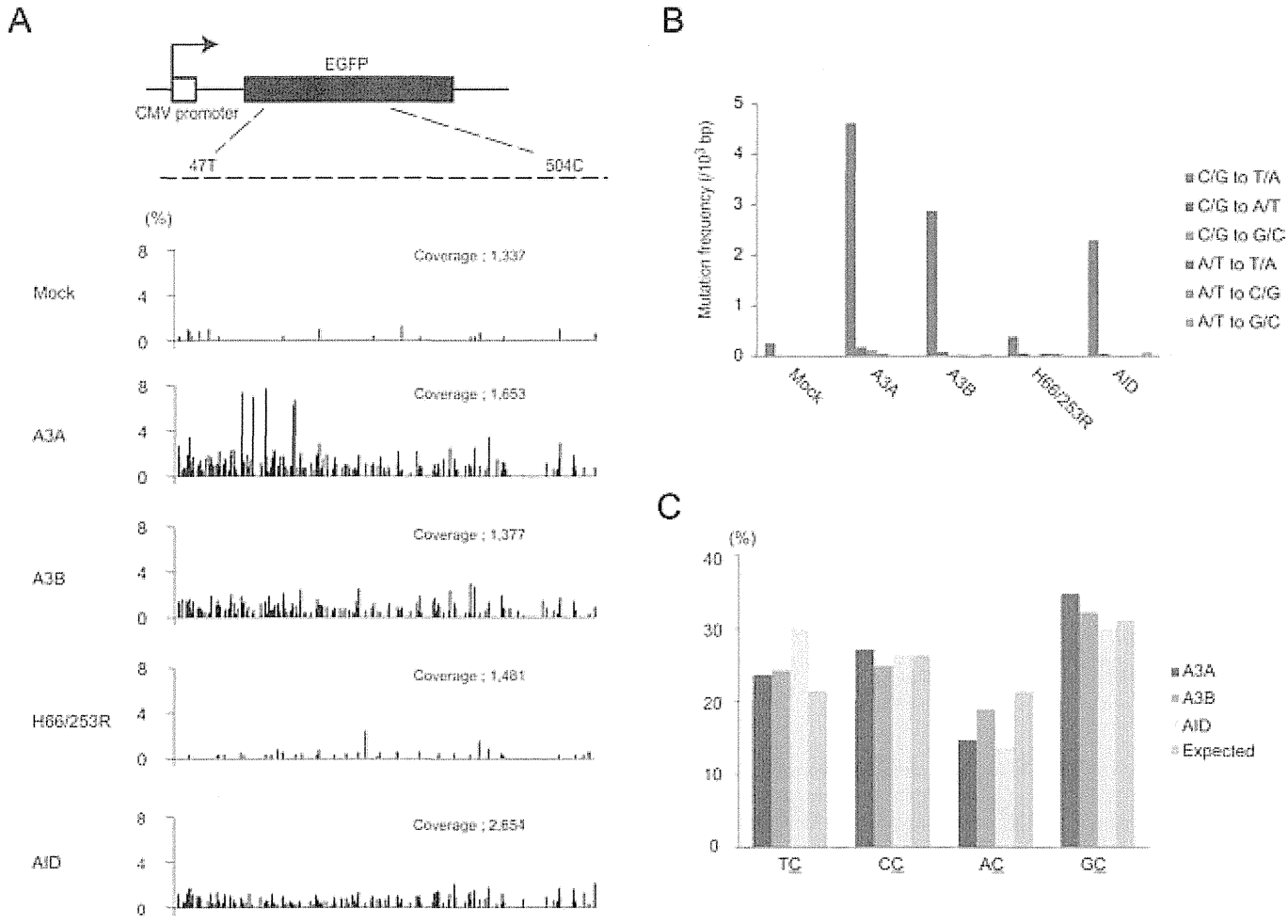

Figure 4 | Deep sequencing of *EGFP* genes in genomic DNA. (A) The distributions of C/G to T/A substitutions in the *EGFP* sequences. Total DNA was recovered form HEK293/EGFP cells 7 days after transfection with expression vector for A3A, A3B wild type or H66/253R or AID. We amplified a portion of *EGFP* sequence from thymine 47 to cytidine 504 (top schematic) by PCR with high-fidelity polymerase and sequenced the amplicons by GS-junior bench top system (Roche). Sequence data were analyzed with equipped software. "Coverage" indicates the total numbers of sequenced reads. (B) Frequencies of base substitutions in hyperedited *EGFP* genes. Base substitutions were classified to 6 groups and substituted base number of each group per 1,000 sequenced base pairs are show. (C) Dinucleotide contexts in genomic DNA editing. The rates of indicated dinucleotide sequence at the C to T transitions are shown. Deviations in the editing contexts do not reach statistical significance ($p < 0.01$) in a χ^2 test.

lymphoma cell lines consistent with prior work suggesting myeloid specificity[25,36]. *AID* transcripts were detected in 2 of 4 cell lines, which is consistent with previous studies[31,32,37]. We also examined expression of *A3B* in two lymph node samples of diffuse large B-cell lymphoma, and found that A3B is actually expressed (supplementary Fig. 3 online).

To investigate the correlation between *A3B* expression and frequency of somatic mutations, we next performed direct sequencing of *cMYC*, *PAX5*, and *A20* genes which are exemplary genes mutated frequently in B-cell lymphoma[33,38]. We compared mutation frequencies of these genes in SUDHL-6 and KIS-1, because the expression of *A3B* was the lowest in the former and the highest in the latter, while AID was not expressed in either cell line. DNA sequences between exon 1 and intron 1 of these three genes were analyzed (899 base pairs of *cMYC*, 1550 base pairs of *Pax5*, and 1088 base pairs of *A20*), since it have been reported that somatic mutations induced by cytidine deaminases were concentrated within 2 kb downstream from transcription initiation sites[33,34]. We found nine mutations within investigated sequences of *cMYC* and *PAX5* in KIS-1, but not in SUDHL-6, in which five of nine mutations detected were C/G to T/A transitions. On the other hand, no mutation was detected within sequenced region of *A20* in either cells (Fig 5b). To analyze ongoing mutations in the genome in individual cells, we next sequenced the same region of *cMYC* sub-cloned from KIS-1 and SUDHL-6, and found several more C to T mutations in KIS-1 cells, but not in SUDHL-6 cells (Supplementary Fig. S4 online). We next determined expression of these tumor-related genes by quantitative RT-PCR and found that the transcripts of *cMYC* and *PAX5* were highly expressed in both SUDHL6 and KIS1 cells as compared to PBL, whereas *A20* was less transcribed in these lymphoma cells. These results suggest that high expression of *A3B* resulted in accumulation of base alterations, especially C/G to T/A transitions, in actively transcribed tumor-related genes in lymphoma cells.

To ascertain more definitely that A3B can edit tumor-related genes in lymphoma cells, we introduced *A3B* into a lymphoma cell line and analyzed somatic mutations in *cMYC*. SUDHL-6 cells were transfected with expression vector for A3B WT, H66/253R, or mock by electroporation and total DNA was extracted after 7-day culture. With 3D-PCR analysis of *cMYC*, we obtained the amplicon from only A3B WT-expressing cells at the lower Td (Fig 6a). Clonal sequencing of amplicons at 85.9°C revealed 2 to 7 nucleotide substitutions per strand, and more than 80% of these mutations were C/G to T/A transitions, with a preference for 5′-GC dinucleotide sites (Fig 6b and c). We also sequenced the amplicons at 94.0°C of Td and

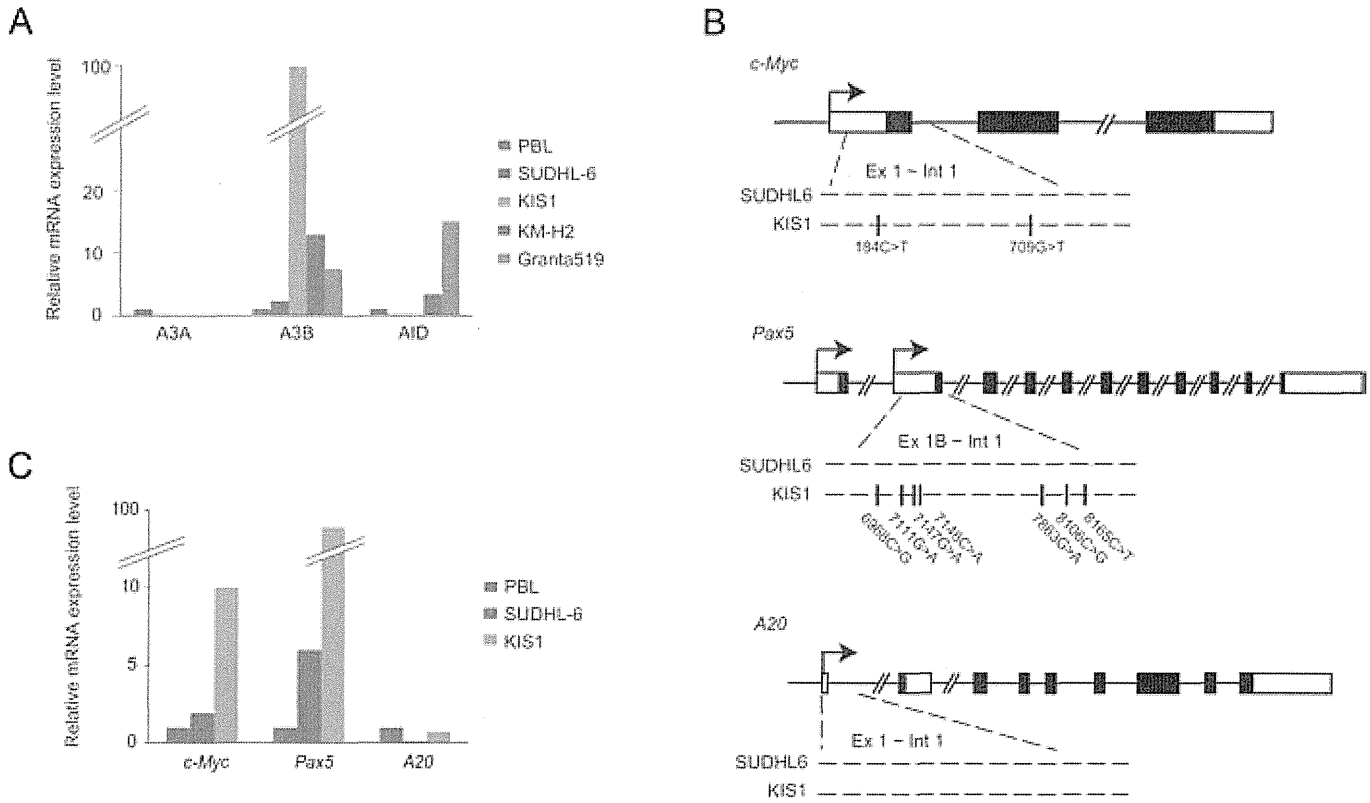

Figure 5 | Expression of *A3B* and somatic mutations in oncogenes in human lymphoma cell lines. (A) Quantitative RT-PCR for *A3A*, *A3B*, and *AID* in lymphoma cell lines. The levels of target cDNA were normalized to the endogenous hypoxanthine phosphoribosyl transferase 1 (*HPRT1*) and then compared to those in peripheral blood lymphocytes. (B) Mutational analyses of *C-myc*, *Pax5*, and *A20* in SUDH6 and KIS1 cells. We recovered total DNA from the cells and amplified the sequence between exon1 and intron1 of *C-myc*, *Pax5* and *A20* by PCR and performed direct sequencing of the amplicons. Locations of somatic mutations are shown below the loci with their positions. (C) The expression levels of transcripts of *C-myc*, *Pax5*, and *A20* in KIS1 and SUDHL6 cells. Quantitative RT-PCR was similarly performed with (a).

found A3B-induced C/G to T/A transitions without 5′-TC dinucleotide preference (supplementary Fig. 5 online). These data demonstrate that expression of A3B can induce somatic mutations into actively transcribed tumor-related genes in lymphoma cells.

Discussion

To date, most studies on A3 proteins have focused on their abilities as antiviral or antitransposon factors, whereas the capability of A3 proteins to induce mutations into genomic DNA in host cells has been scarcely verified. In contrast, many studies have elucidated that AID induces somatic mutations into not only Ig genes, but also tumor-related genes in human cells and that ubiquitous expression of AID in mice leads to cancers of various organs as well as lymphomas, with the accumulation of nucleotides alterations[9–13]. Thus, AID has been considered as the only DNA cytosine deaminase that can induce somatic mutations into human genome and has potential to cause cancers or hematologic malignancies.

Suspène *et al.* have recently reported that hyperediting of both mitochondrial and nuclear DNA was detected in human cells defective for UNG derived from hyper IgM syndrome patients and demonstrated that A3A-induced mutations in nuclear DNA are detectable under the condition of suppressing UNG in human cells[19]. In their report, deamination of nuclear DNA was not observed in cells expressing other A3 proteins or in cells expressing A3A without UNG suppression. Furthermore, Landry *et al.* have reported that expression of A3A together with UGI in mammalian cell lines resulted in breaking of DNA and activation of DNA damage response in a deaminase-dependent manner[18]. In these two reports, the effect on genomic integrity by A3A was dependent on the presence of UGI. Thus, there has been no direct evidence that A3 proteins induce mutations in genomic DNA in the cells with intact DNA repair systems.

In this study, we demonstrate that A3A and A3B as well as AID can induce C/G to T/A transitions into nuclear DNA without suppressing UNG by two different assays, 3D-PCR and deep sequencing. We assume that increased number of cytidine deamination catalyzed by highly expressed A3A or A3B exceeded the processivity of DNA repair enzymes such as UNG and resulted in leaving C/G to T/A transitions in nuclear DNA. Mutation frequencies were considerably lower compared to Suspène's report. However, Yoshikawa *et al.* reported that AID induced hypermutations into an actively transcribed gene in fibroblasts and that the mutation frequency was approximately 4 to 6 per 1000 base pairs[10], almost to the same extent as our results. Hence the frequency of mutations induced by cytidine deaminases into nuclear DNA is probably this extent or less in the cells with intact DNA repair systems.

We also find that *A3B* is highly expressed in several lymphoma cell lines and that the cells expressing high levels of *A3B* actually possesses somatic mutations, especially C/G to T/A transitions, in actively transcribed tumor-related genes. Furthermore, we reveal that introduction of *A3B* into lymphoma cells induces the accumulation of C/G to T/A transitions in *cMYC* gene. This is the first report that suggests the involvement of A3B in inducing somatic mutations of oncogenes in tumor cells. Together with the microarray database of A3B expression in miscellaneous cancer cell lines[14] (NextBio: http://www.nextbio.com), it is possible that A3B may induce somatic mutations into tumor related genes in various types of cancers.

Several questions remain open. First, it remains unclear what is preferred target sequences of A3 proteins in genomic DNA. Because

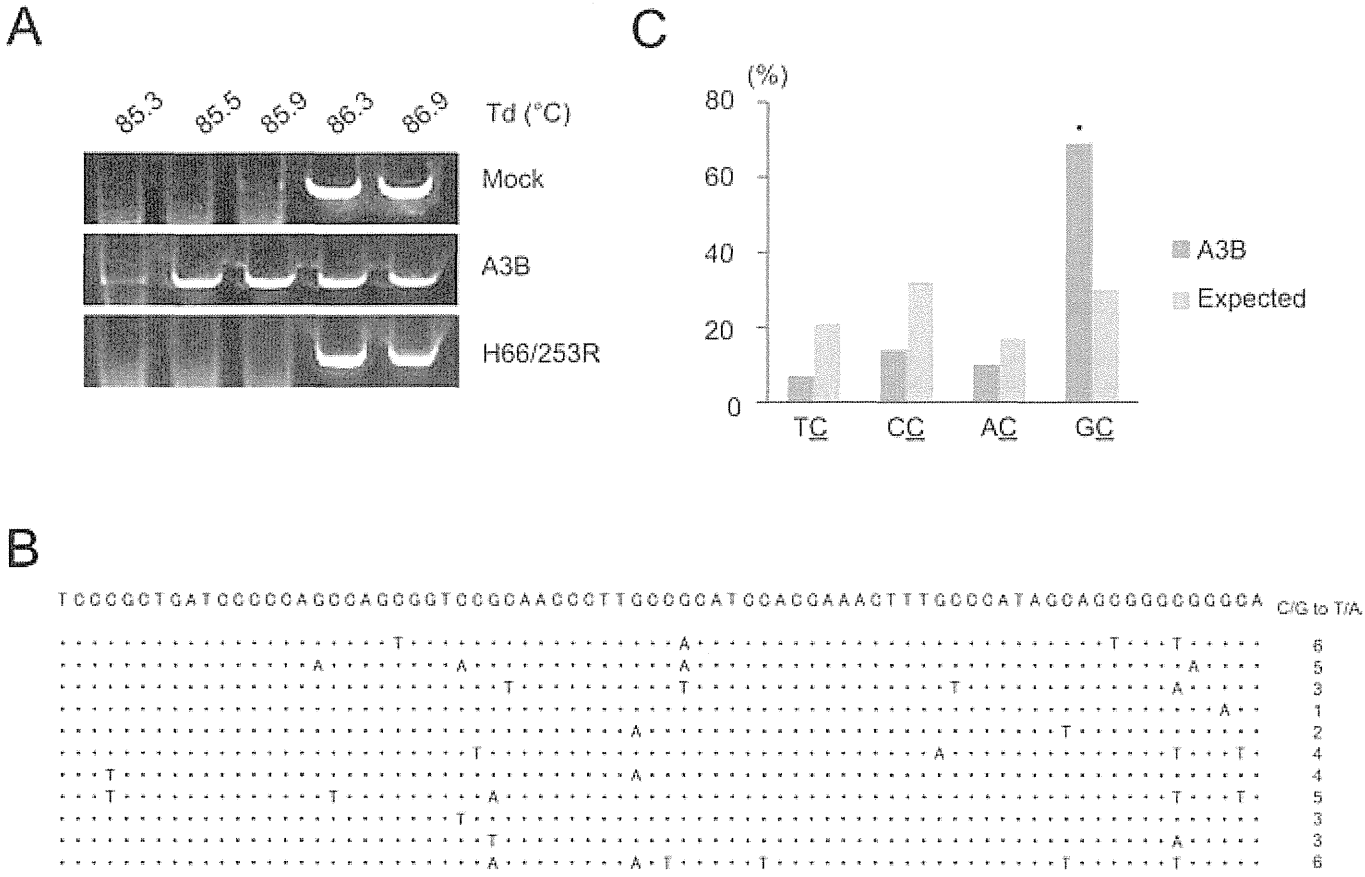

Figure 6 | A3B induced somatic mutations into *c-myc* gene in human lymphoma cells. (A) Agarose gel analyses of 3D-PCR products of *c-Myc* genes in SUDHL6. We transfected expression vector for A3B wild-type or H66/253R or empty vector and recovered total DNA 7 days after transfection. *C-myc* genes were amplified by 3D-PCR at the indicated denaturation temperatures (Td). (B) Clonal sequencing of amplicons from A3B-WT expressing SUDHL6 cells. We sequenced 11 clones (5104 base pairs in total). Seventy six bases from thymine 310 to adenine 385 in which mutations are concentrated among sequenced 464 base pairs are shown. The numbers of C/G to T/A substitutions in sequenced 464 base pair length are shown at the right end. (C) Dinucleotide contexts of somatic mutations in *c-Myc* gene by A3B. The rates of indicated dinucleotide sequence at the C to T transitions are shown. Asterisks indicate statistical significance in a χ^2 test ($p < 0.01$).

in several cancers such as breast cancer and melanoma, 5′-TC is the most prevalent target in C to T base substitutions, A3 is the most potential candidate to induce these mutations[25,28]. However, in our results, neither A3A nor A3B had a definite preference of editing site in nuclear DNA editing, whereas a preference for 5′-TC dinucleotide was observed in foreign DNA editing as previously reported. It is possible that A3A and A3B have no distinct favorite context in nuclear DNA editing, unlike viral and bacterial DNA editing, because human genomic DNA is more profoundly protected in transcription than viral or bacterial DNA and is under survey of DNA repair systems. However, Suspene *et al.* reported that target contexts of cytidine deamination in A3A+UGI-expressing cells were 5′-TC and 5′-CC dinucleotides, which were identical to the contexts of viral or bacterial DNA editing[19]. We assume that this discrepancy might be attributable to cell types or expression levels in cells. Hence, further analyses should be required to clarify the favorite target contexts of A3 proteins in nuclear DNA editing. The second question is how transcriptional control and post-translational modification of A3 proteins regulate A3 activity. Because the molecules that possess a capability of editing nuclear DNA threaten cell homeostasis, expression and activity of A3A and A3B must be strictly controlled. AID is known to be regulated at multiple steps[39], for example, transcriptional regulation[40–42], post-transcriptional regulation by micro-RNA[43,44], regulation of intracellular localization[45,46], and phosphorylation by PKA[47,48]. In contrast to AID, little is known about how A3 proteins are regulated. It has been reported that A3A is abundantly expressed in CD14+ monocytes and upregulated by interferon-α stimulation[25,49,50]. Meanwhile, it is not clear where A3B is expressed normally[25,42,49,50] and how it is regulated. As for post-translational modification, we previously reported that PKA-mediated phosphorylation of A3G regulates the interaction between A3G and HIV Vif[51]. To better understand the physiological roles of A3 proteins, it is important to elucidate how their expression and activity are regulated. The last question is whether A3 proteins can serve as an "initiator" of tumorigenesis. Our results suggest A3B indeed induces somatic mutations into genomic DNA in various human tumor cells, however, it is unclear whether A3B proteins impair genomic DNA from the early stage of oncogenesis. To address this question, hereafter, histopathological and genetic analyses of transgenic mouse constitutively expressing A3 proteins are necessary.

In conclusion, our findings provides the first evidence that A3A and A3B can induce C/G to T/G transitions into genomic DNA without suppressing DNA repair system. Our data also show that high expression of *A3B* is related to mutation frequencies of oncogenes in lymphoma cells. Our results suggest that *A3B* is an oncogene, like AID, which may have the capacity to evoke genomic instability through base substitutions in human cells. Further studies will be required to test whether endogenous A3B is capable of impairing genomic integrity as a DNA mutator and contributing to the development of human cancers and hematologic malignancies.

Methods

DNA constructs and cell lines. Plasmids containing coding sequence of human *A3A* and *A3B* were kindly provided by Dr. Kenzo Tokunaga[21]. Expression vectors for HA-tagged A3A, A3B and AID were generated by sub-cloning of coding sequences into pCAG-GS vector. A3B catalytic domain mutants (H66R, H253R, and H66/253R) were generated by KOD-plus mutagenesis Kit (Toyobo). Expression vector for Uracil-DNA glycosylase inhibitor, pEF-UGI was kindly provided by Dr. Ruben S Harris[25]. HEK293 and HEK293T cells were maintained with Dulbecco's modified Eagle's medium containing 10% of fetal bovine serum (FBS) and penicillin, streptomycin, and glutamine (PSG). All B-cell lymphoma cell lines were maintained with RPMI1640 containing 10% FBS and PSG. Retrovirus containing *EGFP* sequence was produced by co-transfection of pMLV gag-pol, VSV-G, and pDON-EGFP into HEK293T cells. HEK293/EGFP cells were generated by retroviral transduction of *EGFP* and selection of 1 mg/ml G418 for two months.

Immunoblotting. HEK293 cells were transfected with expression vector for A3A, A3B wild-type or mutant (H66R, H253R or H66/253R) or AID, and lysed with RIPA buffer (50 mM Tris-HCl pH7.5, 150 mM NaCl, 1 mM EDTA, 1% Triton-X, 0.1% SDS, 0.1% DOC) after 2-day culture. After centrifugation at 20,000 x g for 15 min, supernatant was mixed with sample buffer (Biorad), boiled for 5 minutes, resolved on 12% (w/v) polyacrylamide gel, transferred to PVDF membrane (Immobilon, Millipore), and analyzed by standard immunoblotting procedure with anti-HA monoclonal antibody (12CA5, Roche) or anti-β-actin monoclonal antibody (AC-15, Sigma).

3D-PCR and clonal sequencing. For foreign DNA editing assay, HEK293 cells were transfected with pEGFP-N3, pEF-UGI, and expression vector for A3A, A3B WT or mutant, or AID by using Fugene HD (Roche). After two-day culture, total DNA was extracted by using Quick Gene DNA whole blood kit (Fuji Film). First round PCR was performed with primers listed in Supplementary Table S2 using rTaq DNA polymerase (Takara), with the following reaction profile; 30 s at 94°C, 25cycles of 30 s at 94°C, 40 s at 62°C, and 90 s at 72°C followed by 10 min at 72°C. The amplicons were separated by electrophoresis on 1% (w/v) agarose gel, and extracted from the gel using Qiaquick Gel Extraction kit (Qiagen). We used 25 ng of first-round PCR products as template for nested PCR using Hotstar Hifidelity DNA polymerase (Qiagen), with the following reaction profile; 5 min at 95°C, 35 cycles of 15 s at 83–92°C, 60 s at 62°C, 80 s at 72°C, followed by 10 min at 72°C. The amplicons derived at 83.8°C were cloned into pT7-blue vector (Novagen). For nuclear DNA editing assay, HEK293/EGFP cells were transfected with expression vector for A3A, A3B WT or mutants, or AID using Fugene HD (Roche). Seven days after transfection, we extracted total DNA from these cells with the same method of foreign DNA editing assay. First round PCR was performed using Advantage HF2 polymerase kit (Clontech), with the following reaction profile;1 min at 94°C, 30 cycles of 30 s at 94°C followed by 2 min at 68°C, followed by 3 min at 68°C. We used 25 ng of first-round PCR products for nested PCR using Hotstar Hifidelity DNA polymerase (Qiagen) with the following reaction profile; 5 min at 95°C, 35 cycles of 15 s at 86–89°C, 60 s at 62°C, and 80 s at 72°C, followed by 10 min at 72°C. The amplicons derived at 86.5°C and 83.8°C were cloned into pT7-blue vector (Novagen). For *c-myc* gene editing assay in lymphoma cells, we transfected SUDHL6 cells with expression vectors for A3B WT or H66/253R by electroporation using Nucleofector (Amaxa) and extracted total DNA from the cells 7 days after transfection. First round PCR and gel extractions of amplicons were performed with the same methods of nuclear DNA editing assay. We used 25 ng of first-round PCR products for nested PCR using Hotstar Hifidelity DNA polymerase (Qiagen), with the following reaction profile; 5 min at 95°C, 35 cycles of 15 s at 85–88°C, 60 s at 62°C, 80 s at 72°C, followed by 10 min at 72°C. The amplicons derived at 85.3°C were cloned into pT7-blue vector (Novagen) and sequenced using 3130xl Genetic Analyzer (Applied Biosystems).

Deep sequencing. Total DNA was extracted from HEK293/EGFP transfected with expression vectors for A3A, A3B WT or H66/253R or AID 7 days after transfection. A portion of *EGFP* gene with 443 base pair length, from thymine 56 to cytosine 498, was amplified with the primers listed in Supplementary Table 2 using Advantage HF2 polymerase kit (Clontech), with the following reaction profile; 1 min at 94°C, 30 cycles of 30 s at 94°C followed by 2 min at 68°C, and followed by 3 min at 68°C. The amplicons were separated by electrophoresis on 1% (w/v) agarose gel, and extracted from the gel using Quiaquick Gel Extraction Kit (Qiagen). Purified amplicons were sequenced using GS junior bench top system (Roche) according to the manufacturer's protocol and analyzed with equipped software, GS Amplicon Variant Analyzer.

Lymphoma cell lines and patient samples. Four B-cell lymphoma cell lines (SUDHL6, KIS1, KM-H2, and Granta519) were cultured in RPMI1640 containing 10% of fetal bovine serum (FBS) and penicillin, streptomycin, and glutamine (PSG). We extracted total DNA from these cells by using Quick Gene DNA whole blood kit (Fuji Film) and total RNA by using mir Vana miRNA isolation kit (Ambion). Tumor biopsy specimens prior to treatment were obtained from two patients with diffuse large B-cell lymphoma. The study was approved by the Kyoto University Institutional Review Board and written informed consent was obtained from each patient. Total RNA were extracted similarly to lymphoma cell lines. Naïve B-cells were isolated from healthy donor's peripheral blood by using MACS® naive B cell isolation kit (Miltenyi Biotec).

Quantitative RT-PCR. Complementary DNA was synthesized from 200 ng of total RNA using Revertra Ace qPCR RT Master Mix (Toyobo). Real-time PCR were performed with Thunderbird SYBR qPCR Mix (Toyobo) according to manufacturer's protocol. Target cDNAs were normalized to the endogenous expression level of the house keeping reference gene for hypoxanthine-guanine phosphoribosyl transferase 1 (*HPRT1*) or glyceraldehyde 3-phosphate dehydrogenase (*GAPDH*). All primers for real-time PCR are listed in Supplementary Table 2.

Sequencing of oncogenes from lymphoma cell lines. We amplified portions of *C-myc*, *Pax5*, and *A20* from with the primers listed in Supplementary Table 2 using Advantage HF2 polymerase kit (Clontech), with the following reaction profile; 1 min at 94°C, 30 cycles of 30 s at 94°C followed by 4 min at 68°C, and followed by 3 min at 68°C. The amplicons were separated by electrophoresis on 1% (w/v) agarose gel, extracted from the gel using Qiaquick Gel Extraction kit (Qiagen), and sequenced using 3130xl Genetic Analyzer (Applied Biosystems). In *c-Myc* clonal sequencing, the amplicon was subcloned into pTA2-vector (TOYOBO) and subsequently sequenced.

1. Hahn, W. C. & Weinberg, R. A. Rules for making human tumor cells. *N Engl J Med* **347**, 1593–603 (2002).
2. Pleasance, E. D. *et al.* A comprehensive catalogue of somatic mutations from a human cancer genome. *Nature* **463**, 191–6 (2010).
3. Bronner, C. E. *et al.* Mutation in the DNA mismatch repair gene homologue hMLH1 is associated with hereditary non-polyposis colon cancer. *Nature* **368**, 258–61 (1994).
4. Greenman, C. *et al.* Patterns of somatic mutation in human cancer genomes. *Nature* **446**, 153–8 (2007).
5. Prickett, T. D. *et al.* Analysis of the tyrosine kinome in melanoma reveals recurrent mutations in ERBB4. *Nat Genet* **41**, 1127–32 (2009).
6. Macduff, D. A. & Harris, R. S. Directed DNA deamination by AID/APOBEC3 in immunity. *Curr Biol* **16**, R186–9 (2006).
7. Conticello, S. G. The AID/APOBEC family of nucleic acid mutators. *Genome Biol* **9**, 229 (2008).
8. Muramatsu, M. *et al.* Class switch recombination and hypermutation require activation-induced cytidine deaminase (AID), a potential RNA editing enzyme. *Cell* **102**, 553–63 (2000).
9. Matsumoto, Y. *et al.* Helicobacter pylori infection triggers aberrant expression of activation-induced cytidine deaminase in gastric epithelium. *Nat Med* **13**, 470–6 (2007).
10. Yoshikawa, K. *et al.* AID enzyme-induced hypermutation in an actively transcribed gene in fibroblasts. *Science* **296**, 2033–6 (2002).
11. Okazaki, I. M. *et al.* Constitutive expression of AID leads to tumorigenesis. *J Exp Med* **197**, 1173–81 (2003).
12. Pasqualucci, L. *et al.* AID is required for germinal center-derived lymphomagenesis. *Nat Genet* **40**, 108–12 (2008).
13. Endo, Y. *et al.* Activation-induced cytidine deaminase links between inflammation and the development of colitis-associated colorectal cancers. *Gastroenterology* **135**, 889–98, 898 e1-3 (2008).
14. Jarmuz, A. *et al.* An anthropoid-specific locus of orphan C to U RNA-editing enzymes on chromosome 22. *Genomics* **79**, 285–96 (2002).
15. Goila-Gaur, R. & Strebel, K. HIV-1 Vif, APOBEC, and intrinsic immunity. *Retrovirology* **5**, 51 (2008).
16. Mangeat, B. *et al.* Broad antiretroviral defence by human APOBEC3G through lethal editing of nascent reverse transcripts. *Nature* **424**, 99–103 (2003).
17. Bogerd, H. P. *et al.* Cellular inhibitors of long interspersed element 1 and Alu retrotransposition. *Proc Natl Acad Sci U S A* **103**, 8780–5 (2006).
18. Landry, S., Narvaiza, I., Linfesty, D. C. & Weitzman, M. D. APOBEC3A can activate the DNA damage response and cause cell-cycle arrest. *EMBO Rep* **12**, 444–50 (2011).
19. Suspène, R. *et al.* Somatic hypermutation of human mitochondrial and nuclear DNA by APOBEC3 cytidine deaminases, a pathway for DNA catabolism. *Proc Natl Acad Sci U S A* **108**, 4858–63 (2011).
20. Lackey, L. *et al.* APOBEC3B and AID have similar nuclear import mechanisms. *J Mol Biol* **419**, 301–14 (2012).
21. Kinomoto, M. *et al.* All APOBEC3 family proteins differentially inhibit LINE-1 retrotransposition. *Nucleic Acids Res* **35**, 2955–64 (2007).
22. Bogerd, H. P., Wiegand, H. L., Doehle, B. P. & Cullen, B. R. The intrinsic antiretroviral factor APOBEC3B contains two enzymatically active cytidine deaminase domains. *Virology* **364**, 486–93 (2007).
23. Suspène, R. *et al.* Extensive editing of both hepatitis B virus DNA strands by APOBEC3 cytidine deaminases in vitro and in vivo. *Proc Natl Acad Sci U S A* **102**, 8321–6 (2005).
24. Bonvin, M. & Greeve, J. Effects of point mutations in the cytidine deaminase domains of APOBEC3B on replication and hypermutation of hepatitis B virus in vitro. *J Gen Virol* **88**, 3270–4 (2007).
25. Stenglein, M. D., Burns, M. B., Li, M., Lengyel, J. & Harris, R. S. APOBEC3 proteins mediate the clearance of foreign DNA from human cells. *Nat Struct Mol Biol* **17**, 222–9 (2010).
26. Suspène, R., Henry, M., Guillot, S., Wain-Hobson, S. & Vartanian, J. P. Recovery of APOBEC3-edited human immunodeficiency virus G->A hypermutants by differential DNA denaturation PCR. *J Gen Virol* **86**, 125–9 (2005).

27. Vartanian, J. P. *et al.* Massive APOBEC3 editing of hepatitis B viral DNA in cirrhosis. *PLoS Pathog* **6**, e1000928 (2010).
28. Bishop, K. N. *et al.* Cytidine deamination of retroviral DNA by diverse APOBEC proteins. *Curr Biol* **14**, 1392–6 (2004).
29. Harris, R. S. *et al.* DNA deamination mediates innate immunity to retroviral infection. *Cell* **113**, 803–9 (2003).
30. Beale, R. C. *et al.* Comparison of the differential context-dependence of DNA deamination by APOBEC enzymes: correlation with mutation spectra in vivo. *J Mol Biol* **337**, 585–96 (2004).
31. Greeve, J. *et al.* Expression of activation-induced cytidine deaminase in human B-cell non-Hodgkin lymphomas. *Blood* **101**, 3574–80 (2003).
32. Deutsch, A. J. *et al.* MALT lymphoma and extranodal diffuse large B-cell lymphoma are targeted by aberrant somatic hypermutation. *Blood* **109**, 3500–4 (2007).
33. Pasqualucci, L. *et al.* Hypermutation of multiple proto-oncogenes in B-cell diffuse large-cell lymphomas. *Nature* **412**, 341–6 (2001).
34. Kotani, A. *et al.* A target selection of somatic hypermutations is regulated similarly between T and B cells upon activation-induced cytidine deaminase expression. *Proc Natl Acad Sci U S A* **102**, 4506–11 (2005).
35. Smit, L. A. *et al.* Expression of activation-induced cytidine deaminase is confined to B-cell non-Hodgkin's lymphomas of germinal-center phenotype. *Cancer Res* **63**, 3894–8 (2003).
36. Chen, H. *et al.* APOBEC3A is a potent inhibitor of adeno-associated virus and retrotransposons. *Curr Biol* **16**, 480–5 (2006).
37. Mottok, A., Hansmann, M. L. & Bräuninger, A. Activation induced cytidine deaminase expression in lymphocyte predominant Hodgkin lymphoma. *J Clin Pathol* **58**, 1002–4 (2005).
38. Kato, M. *et al.* Frequent inactivation of A20 in B-cell lymphomas. *Nature* **459**, 712–6 (2009).
39. Delker, R. K., Fugmann, S. D. & Papavasiliou, F. N. A coming-of-age story: activation-induced cytidine deaminase turns 10. *Nat Immunol* **10**, 1147–53 (2009).
40. Crouch, E. E. *et al.* Regulation of AID expression in the immune response. *J Exp Med* **204**, 1145–56 (2007).
41. Gonda, H. *et al.* The balance between Pax5 and Id2 activities is the key to AID gene expression. *J Exp Med* **198**, 1427–37 (2003).
42. Pauklin, S., Sernández, I. V., Bachmann, G., Ramiro, A. R. & Petersen-Mahrt, S. K. Estrogen directly activates AID transcription and function. *J Exp Med* **206**, 99–111 (2009).
43. Teng, G. *et al.* MicroRNA-155 is a negative regulator of activation-induced cytidine deaminase. *Immunity* **28**, 621–9 (2008).
44. de Yébenes, V. G. *et al.* miR-181b negatively regulates activation-induced cytidine deaminase in B cells. *J Exp Med* **205**, 2199–206 (2008).
45. Ito, S. *et al.* Activation-induced cytidine deaminase shuttles between nucleus and cytoplasm like apolipoprotein B mRNA editing catalytic polypeptide 1. *Proc Natl Acad Sci U S A* **101**, 1975–80 (2004).
46. Patenaude, A. M. *et al.* Active nuclear import and cytoplasmic retention of activation-induced deaminase. *Nat Struct Mol Biol* **16**, 517–27 (2009).
47. Basu, U. *et al.* The AID antibody diversification enzyme is regulated by protein kinase A phosphorylation. *Nature* **438**, 508–11 (2005).
48. McBride, K. M. *et al.* Regulation of class switch recombination and somatic mutation by AID phosphorylation. *J Exp Med* **205**, 2585–94 (2008).
49. Koning, F. A. *et al.* Defining APOBEC3 expression patterns in human tissues and hematopoietic cell subsets. *J Virol* **83**, 9474–85 (2009).
50. Berger, G. *et al.* APOBEC3A is a specific inhibitor of the early phases of HIV-1 infection in myeloid cells. *PLoS Pathog* **7**, e1002221 (2011).
51. Shirakawa, K. *et al.* Phosphorylation of APOBEC3G by protein kinase A regulates its interaction with HIV-1 Vif. *Nat Struct Mol Biol* **15**, 1184–91 (2008).

Acknowledgments

We thank R. Harris for thoughtful feedback and for UGI vector, and K. Tokunaga for A3A and A3B vectors.

Author contributions

M.S. performed most of the experiments, analyzed the data and wrote the manuscript; I.K., M.M., T.S. and K.T. performed sequencing of lymphoma cell lines; K.S. and N.K. wrote the manuscript; M.K. established q-PCR; A.T.K. designed the experiments and wrote the manuscript.

Additional information

Supplementary information accompanies this paper at http://www.nature.com/scientificreports

Competing interest statements: The authors declare no competing financial interests.

How to cite this article: Shinohara, M. *et al.* APOBEC3B can impair genomic stability by inducing base substitutions in genomic DNA in human cells. *Sci. Rep.* 2, 806; DOI:10.1038/srep00806 (2012).

Eur. J. Immunol. 2013. 43: 93–103 DOI: 10.1002/eji.201242699 Cellular immune response 93

European Journal of Immunology

The tyrosine kinase inhibitor dasatinib suppresses cytokine production by plasmacytoid dendritic cells by targeting endosomal transport of CpG DNA

Haruyuki Fujita[1], Toshio Kitawaki[1], Takayuki Sato[1], Takahiro Maeda[2], Shimeru Kamihira[3], Akifumi Takaori-Kondo[1] and Norimitsu Kadowaki[1,4]

[1] Department of Hematology and Oncology, Graduate School of Medicine, Kyoto University, Kyoto, Japan
[2] Department of Island and Community Medicine, Nagasaki University Graduate School of Biomedical Sciences, Nagasaki, Japan
[3] Department of Laboratory Medicine, Nagasaki University Graduate School of Biomedical Sciences, Nagasaki, Japan
[4] Japan Science and Technology Agency, Core Research for Evolutional Science and Technology (CREST), Tokyo, Japan

Plasmacytoid dendritic cells (pDCs) produce a vast amount of interferon (IFN)-α in response to nucleic acids from viruses and damaged self-cells through Toll-like receptor (TLR)7 and TLR9. Pharmaceutical agents that suppress IFN-α production by pDCs are instrumental in elucidating the mechanisms behind IFN-α production, and in developing novel therapies for inflammatory disorders that involve pDCs. Here, we show that a tyrosine kinase inhibitor for chronic myeloid leukemia with multiple targets, dasatinib, strongly suppresses production of IFN-α and proinflammatory cytokines by human pDCs stimulated with multimeric CpG oligodeoxynucleotides (CpG-A) without reducing viability. In contrast, other tyrosine kinase inhibitors, imatinib, and nilotinib, did not suppress the cytokine production at clinically relevant concentrations. Inhibitors of SRC family kinases (SFKs), which are prominent targets of dasatinib, also suppressed the cytokine production. Notably, however, dasatinib, but not SFK inhibitors, abrogated prolonged localization of CpG-A in early endosomes, which is a critical step for pDCs to produce a large amount of IFN-α. This study suggests that dasatinib suppresses IFN-α production by pDCs by inhibiting SFK-dependent pathways and SFK-independent endosomal retention of CpG DNA. Kinases controlling the distinctive endosomal trafficking in pDCs may be exploited as targets to develop novel therapies for pDC-related inflammatory disorders.

Keywords: Dasatinib · Interferon · Plasmacytoid dendritic cells (pDCs) · TLR9

Additional supporting information may be found in the online version of this article at the publisher's web-site

Introduction

Plasmacytoid DCs (pDCs) are a distinctive immune cell type that produces a vast amount of IFN-α in response to virus-derived CpG DNA or ssRNA through TLR9 or TLR7, respectively [1], thus

Correspondence: Dr. Norimitsu Kadowaki
e-mail: kadowaki@kuhp.kyoto-u.ac.jp

playing an important role in antiviral immunity. pDCs also produces IFN-α in response to nucleic acids derived from damaged self-tissues, and are thereby implicated in provoking inflammatory disorders such as lupus and psoriasis [2, 3]. Thus, pharmaceutical agents that suppress IFN-α production by pDCs are instrumental in elucidating mechanisms of the production of a large amount of IFN-α and in developing novel therapies for inflammatory disorders that involve pDCs.

A variety of protein kinases is involved in signaling pathways in immune responses. Antitumor kinase inhibitors that have different targets may be useful to dissect such pathways. Three tyrosine kinase inhibitors (TKIs), imatinib, nilotinib, and dasatinib, have been approved for the treatment of chronic myeloid leukemia (CML) and Philadelphia $(Ph)^+$ acute lymphoblastic leukemia (ALL), which are caused by constitutive activation of an ABL tyrosine kinase [4]. Notably, dasatinib is capable of inhibiting a broad array of tyrosine kinases in addition to ABL, among which SRC family kinases (SFKs) are prominent targets [5]. As a consequence, it has been shown that dasatinib inhibits activation of T cells [6, 7] and NK cells [8, 9] in vitro. However, it has not been reported whether dasatinib affects immunostimulatory activity of DCs, which play a pivotal role in the induction of innate and adaptive immune responses.

Here, we investigated the effect of dasatinib on human pDCs in comparison with the effects of the other TKIs, imatinib, and nilotinib [10]. We show that clinically relevant concentrations of dasatinib, but not imatinib or nilotinib, strongly suppressed the production of IFN-α and proinflammatory cytokines by pDCs without impairing viability. Mechanistic analysis suggests that dasatinib suppresses IFN-α production by pDCs through inhibiting both SFK-dependent pathways and SFK-independent endosomal retention of CpG DNA, which is a critical step for pDCs to produce a large amount of IFN-α [11, 12]. These results have significant implications for dissecting the mechanisms of IFN-α production by pDCs and for developing novel therapies for pDC-related inflammatory disorders.

Results

Dasatinib suppresses cytokine production by pDCs stimulated with TLR9 and TLR7 ligands

There are two major types of CpG oligodeoxynucleotides (ODNs), CpG-A, and CpG-B [13]. CpG-A forms large multimeric aggregates, whereas CpG-B are monomeric and do not form such high order structure [14]. CpG-A shares its particle-like physical features with viral particles and an aggregated self-DNA-antimicrobial peptide complex observed in psoriatic lesions [15]. These particle-like nucleic acids induce pDCs to produce a large amount of IFN-α due to their prolonged retention in early endosomes [11, 12]. Thus, we first examined whether dasatinib suppresses IFN-α production by pDCs stimulated with two TLR9 ligands, ODN2216 (CpG-A) or HSV-1. We also stimulated pDCs with a TLR7 ligand, influenza virus, which similarly induces a large amount of IFN-α production by pDCs. When we stimulated PBMCs depleted of pDCs with ODN2216, IFN-α was scarcely detected in the supernatant (Supporting Information Fig. 1), indicating that pDCs are virtually the only cell type among PBMCs that secretes a detectable level of IFN-α in response to CpG-A. Thus, we pretreated PBMCs for 1 h with one of the three ABL kinase inhibitors dasatinib, imatinib, and nilotinib at clinically relevant concentrations observed in blood after administration. We then added the TLR ligands to each condition and cultured PBMCs for 24 h, and concentrations of IFN-α in the supernatants were measured by ELISA (Fig. 1A). Dasatinib strongly suppressed IFN-α production by pDCs stimulated with ODN2216 as well as natural ligands, HSV-1 or influenza virus, in a dose-dependent manner, and a low concentration (10 nM) was sufficient to induce significant suppression. Imatinib and nilotinib suppressed the IFN-α production to a lesser extent, and high concentrations (5000 and 1000 nM) were necessary to exhibit substantial suppression. When we calculated absolute amounts of IFN-α secreted from a single pDC, we obtained similar results (Supporting Information Fig. 2).

We also examined the effect of dasatinib on IFN-α production by purified pDCs to exclude indirect effects from other cell types. Dasatinib suppressed the production of IFN-α by purified pDCs, whereas imatinib did so to a lesser extent (Fig. 1B), as observed with PBMCs.

Whereas CpG-A induces pDCs to produce both IFN-α and proinflammatory cytokines (TNF-α and IL-6), CpG-B induces production of TNF-α and IL-6 but only a low level of IFN-α [16]. Thus, we next examined whether dasatinib suppresses cytokine production by pDCs stimulated with ODN2216 (CpG-A) or ODN2006 (CpG-B) to compare the suppressive effect of dasatinib on the two types of CpG DNA. Dasatinib strongly suppressed production of IFN-α, TNF-α, and IL-6 induced by ODN2216 (Fig. 1C). In contrast, dasatinib significantly suppressed IFN-α and TNF-α production induced by ODN2006 only at a high concentration (100 nM), and did not suppress IL-6 production (Fig. 1C). Dasatinib reduced the frequency of pDCs bearing intracellular IFN-α and TNF-α (Supporting Information Fig. 3), excluding the possibility that dasatinib simply blocks secretion of the cytokines. In addition, dasatinib suppressed upregulation of CD86 induced by ODN2216 but not by ODN2006 (Supporting Information Fig. 4). Dasatinib also suppressed IL-6 production induced by HSV-1 and influenza virus (Supporting Information Fig. 5).

Neither dasatinib nor imatinib significantly reduced the viability of pDCs stimulated with ODN2216 or ODN2006 (Supporting Information Fig. 6).

Collectively, these data indicate that dasatinib strongly suppresses the production of IFN-α, TNF-α, and IL-6 and the expression of CD86 by pDCs stimulated with CpG-A or natural viral ligands but not with CpG-B without reducing viability.

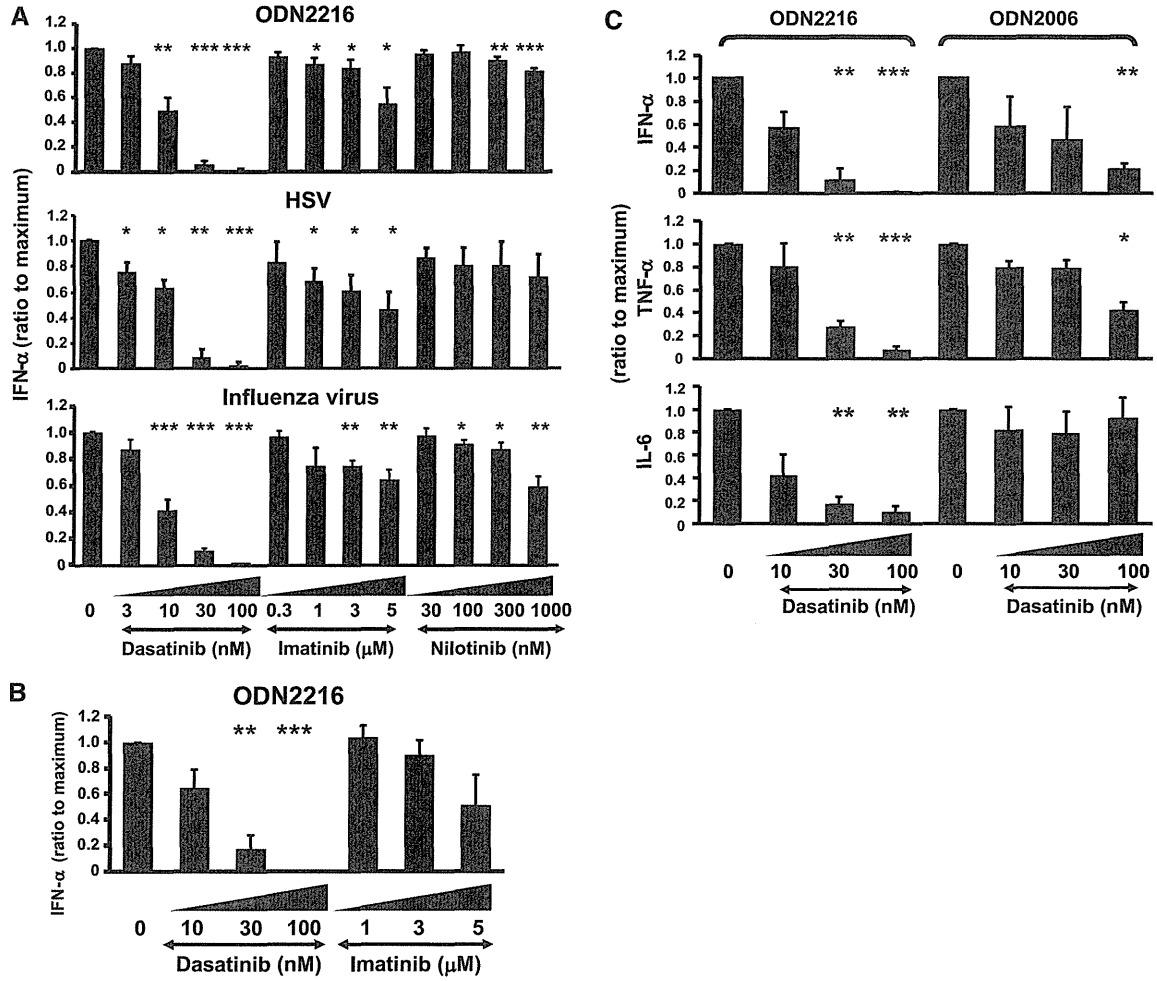

Figure 1. Dasatinib suppresses production of IFN-α and proinflammatory cytokines by pDCs stimulated with CpG-A or viruses. (A) PBMCs were stimulated with ODN2216, HSV-1, or influenza virus in the absence or presence of the indicated concentrations of TKIs for 24 h. The concentration of IFN-α in the supernatants was measured in duplicate by ELISA. Because the absolute concentrations were variable depending on the donors, the cytokine concentrations were normalized to the maximum value obtained without the TKIs. The data are shown as means + SE of 7 (ODN2216), 3 (HSV-1), or 6 (influenza virus) independent experiments. $^{*}p < 0.05$, $^{**}p < 0.01$, $^{***}p < 0.001$ between the data obtained without TKIs and those obtained with each concentration of TKIs, paired two-tailed *t*-test. The means and ranges of absolute concentrations of IFN-α obtained without TKIs are as follows: ODN2216 3874 pg/mL (703–9619 pg/mL); HSV-1 3014 pg/mL (632–5262 pg/mL); influenza virus 5334 pg/mL (2117–10 764 pg/mL). (B) Purified pDCs were stimulated with ODN2216 in the absence or presence of the indicated concentrations of TKIs for 24 h. The concentration of IFN-α in the supernatants was measured in duplicate by ELISA, and normalized to the maximum value obtained without TKIs. The data are shown as means + SE of four experiments. $^{**}p < 0.01$, $^{***}p < 0.001$, paired two-tailed *t*-test. The mean and range of absolute concentrations of IFN-α obtained without TKIs are 62 960 pg/mL (34 078–85 289 pg/mL).(C) Purified pDCs were stimulated with ODN2216 (CpG-A) or ODN2006 (CpG-B) in the absence or presence of the indicated concentrations of dasatinib for 24 h. The concentrations of IFN-α, TNF-α, and IL-6 in the supernatants were measured in duplicate by ELISA, and normalized to the maximum value obtained without dasatinib. The data are shown as means + SE of 4 (IFN-α) and 3 (TNF-α, IL-6) independent experiments. $^{*}p < 0.05$, $^{**}p < 0.01$, $^{***}p < 0.001$, paired two-tailed *t*-test. The means and ranges of absolute concentrations of IFN-α obtained without dasatinib are as follows: ODN2216 62 960 pg/mL (34 078–85 289 pg/mL); ODN2006 398 pg/mL (66–822 pg/mL). TNF-α: ODN2216 1443 pg/mL (1026–1935 pg/mL); ODN2006 849 pg/mL (750–915 pg/mL). IL-6: ODN2216 3883 pg/mL (2173–5160 pg/mL); ODN2006 4156 pg/mL (1483–7571 pg/mL).

Dasatinib reduces the IFN-α-producing capacity of pDCs in vivo

To examine whether administration of dasatinib also reduce the IFN-α-producing capacity of pDCs in vivo, we stimulated PBMCs from patients of CML or Ph^+ ALL with ODN2216 before starting dasatinib (100 mg once a day) or nilotinib (400 mg twice a day) and two time points after starting them, and measured concentrations of IFN-α in the supernatants by ELISA. Because the proportion of pDCs among PBMCs may vary during the clinical course in each patient, we calculated absolute amounts of IFN-α secreted from a single pDC to exclude the influence of fluctuations of the pDC frequency. Information of the patients is described in Supporting Information Table 1. Dasatinib but not nilotinib significantly reduced the IFN-α-producing capacity of pDCs (Fig. 2). This indicates that

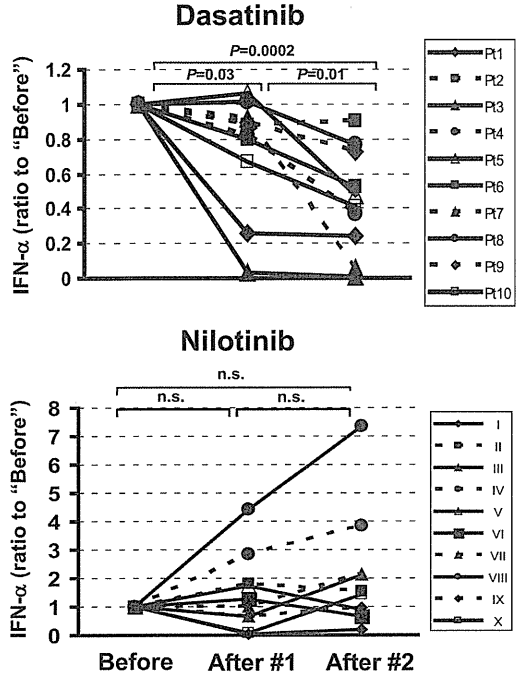

Figure 2. Dasatinib suppresses IFN-α production by pDCs in patients with CML and Ph$^+$ ALL. PBMCs were obtained from 17 CML patients and 3 Ph$^+$ ALL patients (ten patients for dasatinib and nilotinib each) at three time points (before starting dasatinib or nilotinib ("before"), 2–3 weeks after starting the drugs ("after #1"), 4–8 weeks after starting the drugs ("after #2")). PBMCs were stimulated with ODN2216 for 24 h. The concentration of IFN-α in the supernatants was measured by ELISA, and the absolute amounts of IFN-α secreted from a single pDC were calculated. The amounts of IFN-α after starting dasatinib or nilotinib were normalized to the control value obtained before starting them. Statistical significance was determined by paired two-tailed t-test. n.s.: not significant. The means and ranges of the amounts of IFN-α before starting dasatinib or nilotinib are as follows: dasatinib 0.39 pg (0.02–0.92 pg); nilotinib 0.25 pg (0.04–0.63 pg).

dasatinib suppresses the IFN-α-producing capacity of pDCs in vivo as well.

SFK inhibitors suppress IFN-α production by pDCs stimulated with CpG-A

Next, we investigated mechanisms by which dasatinib suppresses cytokine production by pDCs. Because dasatinib strongly suppresses SFKs [5], we examined whether SFK inhibitors PP2 [17] and SU6656 [18], suppress the production of IFN-α, TNF-α, and IL-6 by pDCs stimulated with ODN2216. Whereas PP2 and SU6656 did not significantly reduce the viability of pDCs (data not shown), these reagents suppressed the cytokine production in a dose-dependent manner (Fig. 3A). In contrast, PP2 did not suppress TNF-α and IL-6 production induced by ODN2006, and SU6656 significantly did so only at the highest concentration (Fig. 3B). Thus, it is likely that inhibition of SFKs is responsible for the suppressive effect of dasatinib on pDCs stimulated with CpG-A at least in part.

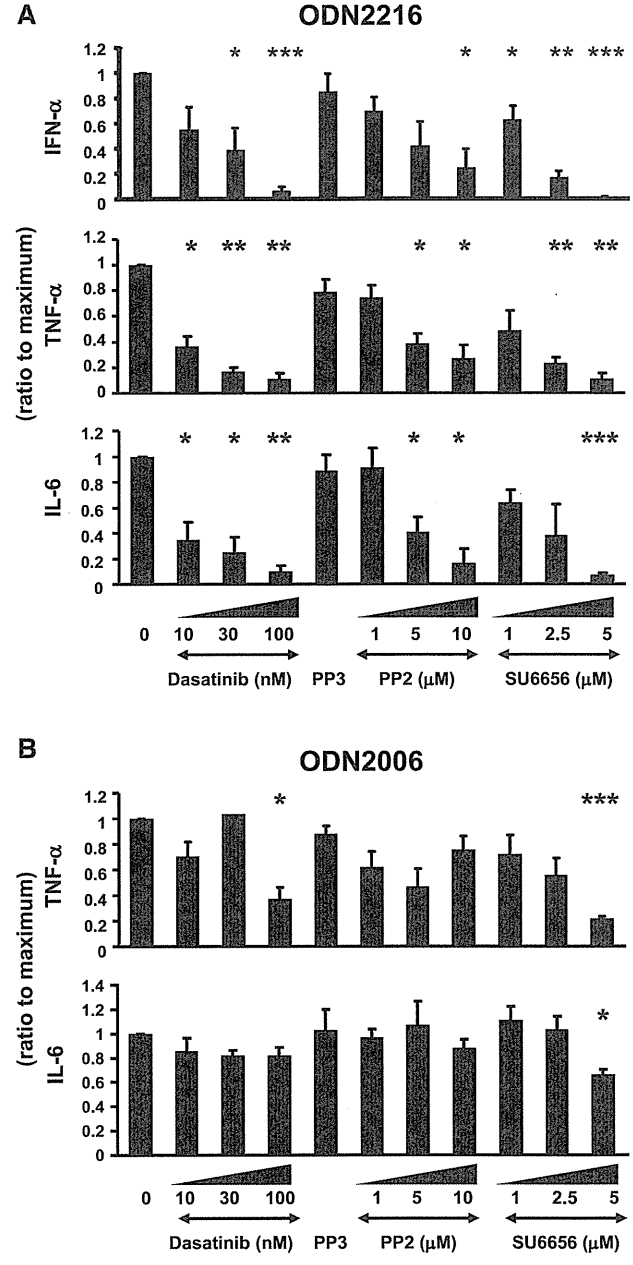

Figure 3. SFK inhibitors suppress production of IFN-α and proinflammatory cytokines by pDCs stimulated with CpG-A. (A) Purified pDCs were stimulated with ODN2216 in the absence or presence of the indicated concentrations of inhibitors or 10 μM PP3 for 24 h. The concentrations of IFN-α, TNF-α, and IL-6 in the supernatants were measured in duplicate by ELISA, and normalized to the maximum value obtained without the inhibitors. The data are shown as means + SE of four (IFN-α) and three (TNF-α, IL-6) experiments. $^*p < 0.05$, $^{**}p < 0.01$, $^{***}p < 0.001$ between data obtained without kinase inhibitors and those obtained with each concentration of inhibitors, paired two-tailed t-test. The mean and range of absolute concentrations of IFN-α, TNF-α, and IL-6 obtained without the inhibitors are 55 157 pg/mL (26 553–12 1608 pg/mL), 421 pg/mL (194–590 pg/mL), and 2059 pg/mL (783–4389 pg/mL), respectively. (B) Purified pDCs were stimulated with ODN2006 in the absence or presence of the inhibitors for 24 h. The concentrations of TNF-α and IL-6 in the supernatants from three experiments were analyzed as in (A). The mean and range of absolute concentrations of TNF-α and IL-6 obtained without the inhibitors are 263 pg/mL (70–598 pg/mL) and 1027 pg/mL (427–1902 pg/mL), respectively.

Dasatinib inhibits nuclear translocation of IRF7 and NF-κB in pDCs stimulated with CpG-A

The earliest event leading to CpG ODN-induced IFN-α production is endocytosis of CpG ODN by pDCs. Thus, we examined whether dasatinib inhibits uptake of CpG ODN by pDCs. We observed the intracellular localization of FITC-conjugated ODN2216 in the absence or presence of dasatinib by confocal microscopy (Supporting Information Fig. 7). Whereas pDCs kept on ice did not endocytose ODN2216, pDC cultured at 37°C did. Dasatinib did not inhibit the endocytosis of ODN2216. Thus, dasatinib targets a signaling pathway(s) further downstream.

Upon stimulation with CpG ODN, TLR9 rapidly moves from the ER to endosomes [19]. We have recently shown that a proteasome inhibitor bortezomib inhibits the intracellular trafficking of TLR9 in pDCs [20]. Thus, we next examined whether dasatinib also inhibits this step. We stimulated purified pDCs with ODN2216 in the absence or presence of dasatinib, and examined whether TLR9 colocalizes with an ER marker (ER-Tracker) or early endosomal markers (EEA1 and Rab5) by confocal microscopy. To quantitatively compare the degrees of colocalization between culture conditions, we analyzed the data using Manders' Colocalization Coefficients [21, 22] with the Costes' method of automatic thresholding [22, 23]. Supporting Information Fig. 8A and B shows representative confocal images and statistical analysis of pooled microscopy data, respectively. TLR9 colocalized with ER-Tracker but not with EEA1 or Rab5 without stimulation. In contrast, TLR9 did not colocalize with ER-Tracker and instead colocalized with EEA1 and Rab5 after stimulation with ODN2216, indicating trafficking of TLR9 from the ER to early endosomes. TLR9 also colocalized with EEA1 and Rab5 but not with ER-Tracker even in the presence of dasatinib. Thus, dasatinib does not inhibit the trafficking of TLR9 from the ER to endosomes induced by CpG ODN.

Stimulation of pDCs with CpG ODN induces the nuclear translocation of two major transcription factors, IFN regulatory factor (IRF)7 and NF-κB [24]. IRF7 and NF-κB induce the production of IFN-α and proinflammatory cytokines at the final step of TLR signaling, respectively. Thus, we examined whether dasatinib inhibits the nuclear translocation of these transcription factors induced by ODN2216 in pDCs. Whereas IRF7 and NF-κB are located in the cytoplasm in untreated pDCs, both of the transcription factors moved to the nucleus after stimulation with ODN2216 (Fig. 4). Dasatinib inhibited the nuclear translocation of IRF7 and NF-κB, consistently with the suppression of production of IFN-α and proinflammatory cytokines induced by ODN2216.

Dasatinib and a SFK inhibitor inhibit intracellular events upstream of TLR9 engagement

Intracellular events after endocytosis of CpG DNA resulting in the nuclear translocation of transcription factors are composed of (i) trafficking of endosomes carrying CpG DNA (upstream of TLR9) and (ii) signaling triggered by TLR9 engagement (downstream

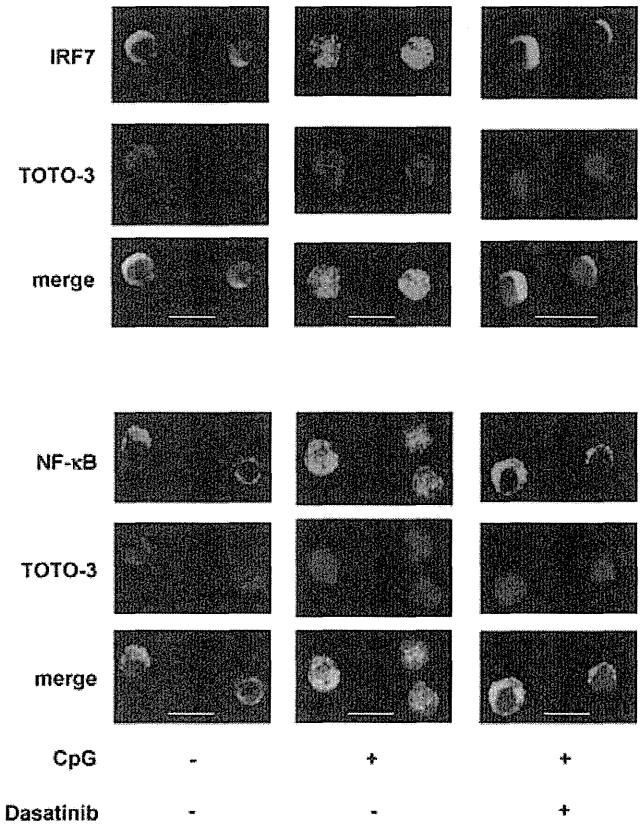

Figure 4. Dasatinib inhibits the nuclear translocation of IRF7 and NF-κB in pDCs.Purified pDCs were stimulated with ODN2216 in the absence or presence of dasatinib for 24 h. The cells were stained with rabbit anti-IRF7 (top) or anti-NF-κBp65 (bottom, both green). Nuclei were identified using TOTO-3 dye (blue). The data shown are representative of three experiments performed. Scale bars, 10 μm.

of TLR9). Chloroquine suppresses CpG-induced cellular activation by inhibiting endosomal acidification and thus cleavage of the ectodomain of TLR9 necessary for downstream signaling [25], resulting in suppression of IFN-α production by pDCs (data not shown). Thus, we compared the effects of the three TKIs, PP2, and chloroquine on CpG-induced IFN-α production and tyrosine phosphorylation in pDCs. Because we could not extract sufficient amounts of proteins from primary pDCs to obtain unambiguous results in Western blotting, we used a cell line derived from blastic pDC neoplasm, CAL-1 [26]. As mixing ODN2216 with cationic liposome 1,2-dioleoyloxy-3-trimethylammonium-propane (DOTAP) was necessary to induce CAL-1 to produce IFN-α, we stimulated CAL-1 with the mixture of ODN2216 and DOTAP. Dasatinib, PP2, and chloroquine suppressed IFN-α production by CAL-1, as they did for primary pDCs (Supporting Information Fig. 9A). The stimulation induced tyrosine phosphorylation of several proteins (Supporting Information Fig. 9B). Chloroquine did not inhibit the phosphorylation, indicating that the tyrosine phosphorylation induced by CpG DNA occurs upstream of TLR9 engagement. In contrast, dasatinib, but not imatinib or nilotinib, inhibited the phosphorylation in a dose-dependent manner. PP2 also did so. These data suggest that dasatinib and PP2 inhibit intracellular events upstream of TLR9.

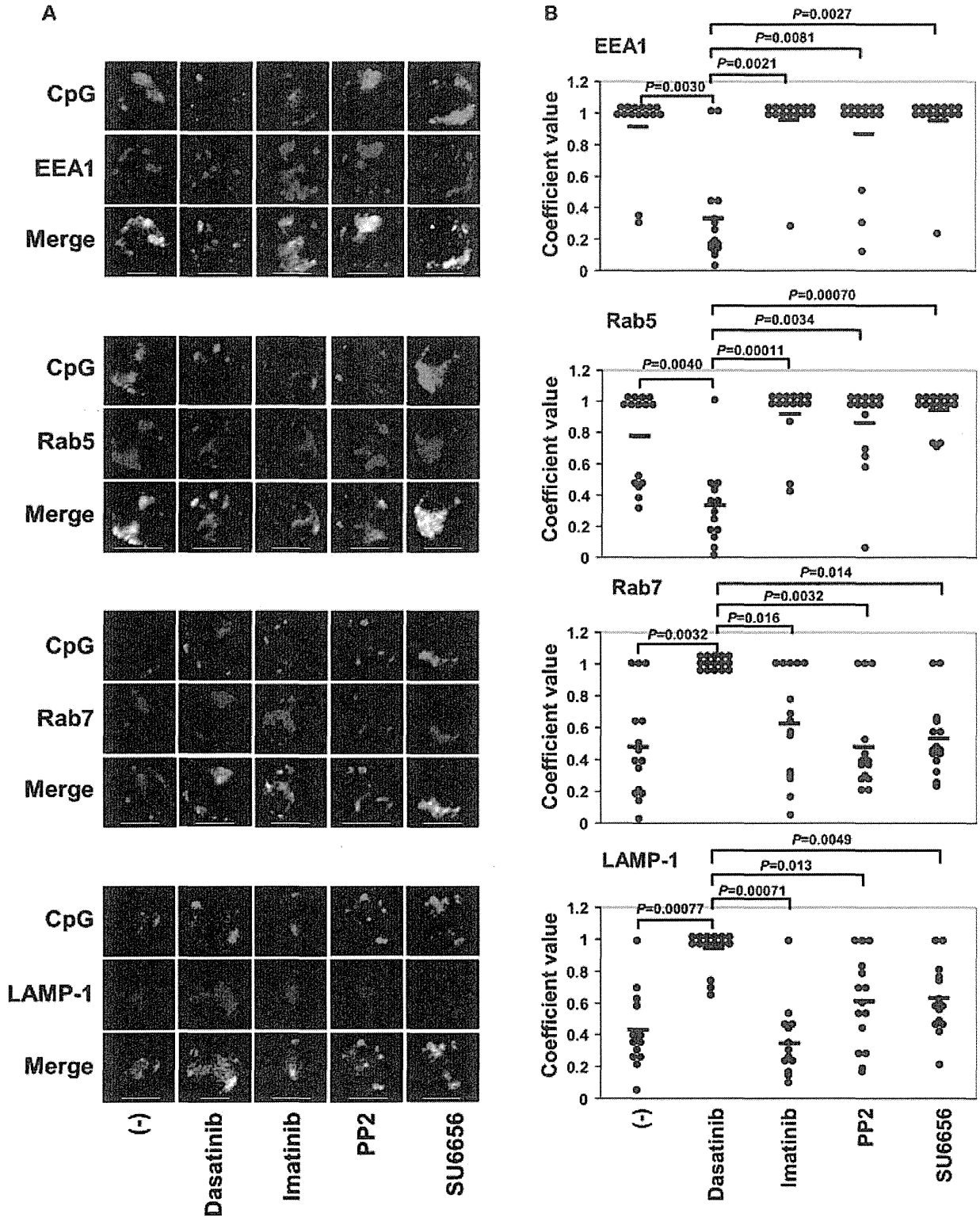

Figure 5. Dasatinib, but not SFK inhibitors, inhibits the retention of CpG-A in early endosomes. Purified pDCs were cultured with FITC-conjugated ODN2216 in the absence or presence of the TKIs or the SFK inhibitors for 90 min. The cells were stained with anti-EEA1 or anti-Rab5 mAb for early endosomes, or anti-Rab7 mAb for late endosomes, followed by Alexa Fluor 555-conjugated goat anti-rabbit IgG. Alternatively, the cells were stained with PE-conjugated mouse anti-LAMP-1 mAb for late endosomes and lysosomes. (A) Data shown are representative of three to five experiments. Positive signals for both probes are shown in white. Scale bars, 5 μm. (B) Statistical analysis of microscopy data pooled from three to –five experiments. Each symbol represents a cell, and 15 cells were analyzed for each condition. The coefficient value represents the fraction of green in compartments containing red. Statistical significance was determined by Mann–Whitney *U*-test with Bonferroni correction following Kruskal–Wallis *H*-test.

Dasatinib, but not SFK inhibitors, abrogates retention of CpG-A in early endosomes

It has been shown that CpG-A is retained in early endosomes together with the MyD88-IRF7 complex for a long period in pDCs but not in conventional DCs [11, 12]. This spatiotemporal regulation of CpG trafficking is likely to enable prolonged activation of the signaling complex, leading to prodigious production of IFN-α by pDCs. Thus, we examined whether the TKIs (dasatinib, imatinib) and the SFK inhibitors (PP2, SU6656) affect trafficking of endosomes carrying CpG-A in pDCs by confocal microscopy. We used EEA1 and Rab5 as early endosome markers, Rab7 as a late endosome marker, and LAMP-1 as a lysosome marker. Figure 5A and B shows representative confocal images and statistical analysis of pooled microscopy data, respectively. ODN2216 colocalized with EEA1 and Rab5 rather than with Rab7 and LAMP-1 without any of the inhibitors, indicating retention of ODN2216 in early endosomes. Notably, ODN2216 colocalized with Rab7 and LAMP-1 rather than with EEA1 and Rab5 in the presence of dasatinib, indicating that dasatinib abrogates the retention of ODN2216 in early endosomes. In contrast, ODN2216 remained colocalized with EEA1 and Rab5 in the presence of imatinib. Unexpectedly, ODN2216 also remained colocalized with EEA1 and Rab5 in the presence of PP2 or SU6656, indicating that the SFK inhibitors as well as imatinib do not abrogate the retention of ODN2216 in early endosomes. Collectively, these data suggest that dasatinib, but not imatinib, abrogates retention of CpG-A in early endosomes and facilitates trafficking to late endosomes and lysosomes in pDCs by inhibiting protein kinases other than SFKs.

Discussion

pDCs represent a unique immune cell type in that they rapidly produce a vast amount of IFN-α in response to nucleic acids derived not only from pathogens but also from damaged self-cells. Here, we showed that a TKI dasatinib potently suppresses IFN-α production by pDCs without reducing cell viability. Importantly, dasatinib abrogated retention of CpG-A in early endosomes and facilitated the movement of CpG-A to late endosomes/lysosomes. It is of note that this effect is independent of SFKs. This is the first study showing the pharmacological interruption of the critical step for pDCs to produce IFN-α: prolonged localization of CpG DNA in early endosomes [11, 12]. It sheds new light on the molecular mechanisms by which pDCs perform their immune functions and on the development of novel therapies for pDC-related inflammatory disorders.

Among the three TKIs (dasatinib, imatinib, nilotinib), dasatinib most strongly suppressed IFN-α production by pDCs stimulated with representative IFN-α inducers, ODN2216 (CpG-A), HSV-1 (TLR9 ligand), or influenza virus (TLR7 ligand) at clinically relevant, low concentrations. Although imatinib and nilotinib also diminished IFN-α production, the effects were much weaker than that of dasatinib and needed high concentrations. Dasatinib also potently suppressed production of TNF-α and IL-6 as well as expression of CD86 by pDCs stimulated with ODN2216 (CpG-A). However, the suppression of such responses induced by ODN2006 (CpG-B) was less marked. The main difference between CpG-A and CpG-B is in the mode of their endosomal transport; CpG-A is retained in early endosomes for a longer time than CpG-B [11, 12]. Thus, the differential effects of dasatinib on the stimulation with CpG-A and CpG-B imply that dasatinib may target certain functions of early endosomes.

Importantly, dasatinib, but not nilotinib, significantly diminished the IFN-α-producing capacity of pDCs in patients treated with these drugs. These data are consistent with the in vitro data, and suggest that dasatinib suppresses the IFN-α-producing capacity of pDCs in vivo as well.

Next, we examined the mechanisms by which dasatinib suppresses cytokine production by pDCs stimulated with CpG-A. Two inhibitors of SFKs (PP2, SU6656) significantly suppressed production of IFN-α, TNF-α, and IL-6 by pDCs stimulated with CpG-A but not with CpG-B, consistent with the previous report [27]. Correspondingly, dasatinib and PP2 suppressed CpG-triggered global tyrosine phosphorylation in a pDC cell line CAL-1, but chloroquine did not, suggesting that dasatinib and PP2 inhibits CpG-induced intracellular events upstream of TLR9. Notably, however, dasatinib but not PP2 or SU6656 abrogated prolonged localization of CpG-A in early endosomes, and facilitated transport of CpG-A to late endosomes/lysosomes. These data suggest that dasatinib suppresses IFN-α production by pDCs through inhibiting both SFK-dependent and SFK-independent signaling pathways. Although both of the pathways appears to be involved in the functions of early endosomes necessary for responses to CpG-A, the data of confocal microscopy indicates that only the SFK-independent pathway is responsible for the prolonged localization of CpG-A in early endosomes.

The mechanisms by which an aggregated form of CpG DNA is retained in early endosomes in pDCs for a long period remain to be elucidated. It has been shown that an aggregated form of CpG DNA rapidly goes to late endosomes/lysosomes in conventional DCs in mice [11], suggesting that pDCs have distinctive mechanisms for retention of CpG DNA in early endosomes. A wide variety of protein kinases is involved in endocytic pathways [28]. Dasatinib targets a broad array of tyrosine kinases and several serine/threonine kinases [29–32]. Thus, dasatinib may affect endosomal trafficking in pDCs by inhibiting certain protein kinases other than SFKs involved in early-to-late endosome transition.

In this context, two recent studies have shown that the machinery of lysosome-related organelle biogenesis is essential for TLR7 and TLR9 signaling in pDCs but not in conventional DCs. Sasai et al [33] have reported that the adaptor protein (AP)-3 complex is responsible for trafficking of TLR9 to $IRF7^+$ endosomes but not to $NF\text{-}\kappa B^+$ endosomes using mouse macrophages, and that AP-3 is necessary for the production of IFN-α but not IL-12 by mouse pDCs. Blasius et al. [34] have reported that an oligopeptide transporter Slc15a4 and three protein complexes involved in Hermansky–Pudlak syndrome (AP-3, biogenesis of lysosome-related organelles complex (BLOC)-1, BLOC-2) are required for production of both IFN-α and proinflammatory cytokines by pDCs

stimulated with TLR7 or TLR9 ligands. Slc15a4 [35] and the three complexes [36] are located in early endosomes, and BLOC-1 is necessary for sorting certain cargoes from early endosomes to lysosome-related organelles [37]. Together with these findings, the present study suggests that distinctive properties of early endosomes in pDCs, which is affected by dasatinib, are crucial for the large amount of IFN-α production. Although vesicle traffic pathways for TLR7 ligands to induce IFN-α has not been reported, the involvement of Slc15a4 [34] and AP-3 [33] in type I IFN production by pDCs stimulated with TLR7 ligands suggests that dasatinib targets similar machineries for IFN-α induction by TLR7 and TLR9 ligands.

In conclusion, dasatinib strongly suppresses the production of IFN-α and proinflammatory cytokines by pDCs stimulated with CpG-A, most likely by inhibiting both SFK-dependent and independent pathways, the latter of which is responsible for the prolonged localization of an aggregated form of CpG DNA in early endosomes. Protein phosphorylation is at the heart of controlling the physical properties of endocytosis and of integrating them with signal transduction networks of the cell [28]. Thus, the present study provides a clue to dissect molecular mechanisms for the distinctive behavior of endosomes in pDCs as well as possibilities to develop novel therapies for inflammatory disorders by targeting the endosomal trafficking in pDCs.

Materials and methods

Culture media and reagents

RPMI 1640 (Wako, Osaka, Japan) supplemented with 10% heat-inactivated FBS (Equitec-Bio, Inc., Kerrville, TX, USA), 2 mM L-glutamine, penicillin G, streptomycin (Gibco BRL, Carlsbad, CA, USA), and 10 mM HEPES (Nacalai Tesque, Kyoto, Japan) were used for cell culture. Dasatinib (provided by Bristol-Myers Squibb Company), imatinib, and nilotinib (provided by Novartis Pharma) were dissolved in DMSO (Nacalai Tesque) at 100 mM as a stock solution and were stored at −20°C. A SFK inhibitor PP2 and its negative control PP3 were purchased from Calbiochem (Darmstadt, Germany), and a SFK inhibitor SU6656 was purchased from Cayman Chemical (Ann Arbor, MI, USA). HSV-1 (KOS strain, a gift from Dr. Masaki Yasukawa (Ehime University, Ehime, Japan)) was attenuated with UV irradiation. Influenza virus ($10^{5.3}$ median tissue culture infective dose/0.2 mL of A/Niigata/05F254/2006, a kind gift from Dr. Reiko Saito (Niigata University, Niigata, Japan)) was inactivated at 56°C for 30 min. A cell line derived from blastic plasmacytoid dendritic cell neoplasm CAL-1 was described previously by Maeda et al. [26].

Isolation of pDCs

This study was approved by the Institutional Review Board of the Graduate School of Medicine at Kyoto University and abides by the tenets of the Declaration of Helsinki. PBMCs were obtained from healthy donors with written informed consent. $CD4^+CD11c^-lin^-$ cells were isolated as pDCs as described [38], using FACSAria cell sorter (BD Biosciences, San Jose, CA, USA). Reanalysis of the sorted cells confirmed a purity of more than 98%.

Cell culture

PBMCs were plated in flat-bottom, 96-well plates at 4×10^5 cells/200 μL. Purified pDCs were plated in round-bottom, 96-well plates at 4×10^4 cells/200 μL, except culture for stimulation with ODN2006 where the cells were plated at 1×10^5 cells/200 μL. The cells were pretreated with indicated concentrations of TKIs or SFK inhibitors for 1 h, and were stimulated with 0.5 μM ODN2216 (CpG-A) [16], ODN2006 (CpG-B) [39] (Operon Biotechnologies, Huntsville, AL, USA), 10^6 PFU/mL HSV-1, or 0.5% vol/vol influenza virus without removing the inhibitors for 24 h. For control culture, DMSO was added instead of the inhibitors. The cells were used for flow cytometry, and the supernatants were used for ELISA. For confocal analyses, pDCs were cultured for indicated time periods.

Analysis of cell viability

The cultured pDCs were stained with FITC-conjugated CELL LAB ApoScreen annexin V (Beckman Coulter, Orange County, CA, USA) and propidium iodide, and were analyzed for viability by flow cytometry with the FACSCalibur, and data were analyzed with CellQuest software (BD Biosciences).

Analysis of cytokine production by ELISA

Concentrations of cytokines in the supernatants were measured by ELISA. The following reagents were used: the human IFN-α module set (Bender MedSystems, Vienna, Austria) and the human TNF-α and IL-6 ELISA MAX Standard sets (BioLegend, San Diego, CA, USA).

Analysis of patient samples

Peripheral blood samples were obtained from 17 CML (chronic phase) patients and three Ph^+ ALL patients who newly started dasatinib or nilotinib, at three time points (before, 2–3 weeks after, and 4–8 weeks after starting dasatinib or nilotinib) under the approval by the Institutional Review Board of the Graduate School of Medicine at Kyoto University and with written informed consent. PBMCs isolated with Lympholyte-H (CEDARLANE, Burlington, Ontario, Canada) were stained with FITC-conjugated

anti-BDCA-2 (CD303) mAb (Miltenyi Biotec, Bergisch Gladbach, Germany), and pDCs were identified as BDCA-2$^+$ cells with the FACSCalibur. Dead cells were excluded by staining with propidium iodide. Absolute numbers of pDCs in the wells were calculated from numbers of PBMCs and percentages of BDCA-2$^+$ cells among PBMCs. The PBMCs were cultured in flat-bottom, 96-well culture plates at 4×10^5 cells/200 μL in the presence of 0.5 μM ODN2216 for 24 h. Culture supernatants were analyzed for concentrations of IFN-α by ELISA. The amounts of IFN-α secreted from a single pDC were calculated by dividing the amounts of IFN-α in the supernatants by absolute numbers of pDCs.

Western blotting

CAL-1 cells were pretreated for 1 h with 10 μM PP3, 10 μM PP2, 10 μM chloroquine (WAKO), 5 μM imatinib, 1 μM nilotinib, or indicated concentrations of dasatinib. The cells were stimulated with DOTAP Liposomal Transfection Reagent (Roche Applied Science, Penzberg, Germany) alone or 1 μM ODN2216 plus DOTAP for 1 h without removing the inhibitors. The cells were lysed directly in sample buffer containing 1%SDS, boiled, and diluted tenfold with 1% Triton X-100-containing lysis buffer. The cell extracts were fractionated by SDS-PAGE and transferred to Immobilon-P transfer membranes (Millipore, Billerica, MA, USA), using a wet transfer apparatus (Bio-Rad Laboratories, Hercules, CA, USA). The membranes were incubated with HRP-conjugated anti-phosphotyrosine mAb (PY20) (Transduction Laboratories, Lexington, KY, USA) or anti-β-actin mAb (Sigma, St. Louis, MO, USA) for 1 h. After a wash with TBS-T (25 mM Tris-HCl (pH 7.4), 137 mM NaCl, 2.7 mM KCl, and 0.1% Tween 20), peroxidase activity was detected with Pierce Western Blotting Substrate (Thermo Scientific, Waltham, MA, USA).

Confocal microscopy

To observe uptake of CpG ODN, purified pDCs were cultured in the absence or presence of 100 nM dasatinib for 1 h, and were incubated with 6 μM FITC-conjugated ODN2216 (InvivoGen, San Diego, CA, USA) for 3 h without removing dasatinib. The cells were harvested, washed, stained with PE-conjugated anti-HLA-DR mAb (BD Biosciences), and fixed with 2% paraformaldehyde. pDCs cultured without dasatinib and with FITC-conjugated ODN2216 on ice were used as a negative control for endocytosis.

To observe translocation of TLR9 from ER to endosomes, pDCs were cultured in the absence or presence of 30 nM dasatinib for 1 h, and were stimulated with 0.5 μM ODN2216 without removing dasatinib for 2 h. ER-Tracker Red (Invitrogen, Carlsbad, CA) was added for 30 min before harvest. After fixation with 4% paraformaldehyde for 5 min at room temperature, permeabilization with 0.1% Triton X-100 for 5 min at −20°C, and blocking with 10% goat serum, the cells were stained with rabbit anti-EEA1 mAb (C45B10) or rabbit anti-Rab5 mAb (C8B1) (Cell Signaling Technology, Danvers, MA, USA) followed by Alexa Fluor 555-conjugated goat anti-rabbit IgG (Cell Signaling Technology), and were stained with biotinylated mouse anti-TLR9 mAb (26C593.2) (IMGENEX, San Diego, CA, USA) followed by Alexa Fluor 488-conjugated streptavidin (Invitrogen).

To observe nuclear translocation of IRF7 and NF-κB, pDCs were cultured in the absence or presence of 30 nM dasatinib for 1 h, and were stimulated with 0.5 μM ODN2216 without removing dasatinib for 3 h. After fixation with 2% paraformaldehyde for 15 min at 37°C, permeabilization with 100% methanol for 10 min at −20°C, and blocking with 10% goat serum, the cells were stained with rabbit anti-IRF7 (sc-9083) or NF-κBp65 (sc-109) polyclonal antibody (Santa Cruz Biotechnology, Santa Cruz, CA, USA) followed by Alexa Fluor 488-conjugated goat-anti rabbit IgG (Invitrogen). Nuclei were identified using TOTO-3 dye (Invitrogen).

To observe intracellular trafficking of CpG ODN, pDCs were cultured in the absence or presence of 30 nM dasatinib, 5 μM imatinib, 10 μM PP2, or 5 μM SU6656 for 1 h, and were incubated with 6 μM FITC-conjugated ODN2216 without removing the inhibitors for 90 min. After fixation with 4% paraformaldehyde for 5 min at room temperature, permeabilization with 0.1% Triton X-100 for 5 min at −20°C, and blocking with 10% goat serum, the cells were stained with anti-EEA1, anti-Rab5 mAb, or rabbit anti-Rab7 XP mAb (D95F2), followed by Alexa Fluor 555-conjugated goat anti-rabbit IgG (Cell Signaling Technology). Alternatively, the cells were stained with PE-conjugated mouse anti-LAMP-1 mAb (BioLegend) after blocking for 30 min using Image-iT FX signal enhancer (Invitrogen).

The cells were attached to slide glass by cytospin centrifuge and examined with an oil immersion objective (×60 Plan Apo, numerical aperture 1.4) by LSM510 META confocal microscope (Carl Zeiss, Oberkochen, Germany). Data were acquired with LMS5 software Version 3.2 (Carl Zeiss).

Colocalization analysis

Images were analyzed with Fiji (http://fiji.sc/wiki/index.php/Fiji), an image-processing package based on ImageJ. Colocalization amounts were analyzed using Manders' Colocalization Coefficients [21, 22] with the Costes' method of automatic thresholding [22, 23] using the Coloc_2 plug-in. The coefficient value represents the fraction of green in compartments containing red.

Statistical analyses

Data are presented as means ± SE. The significance of differences was determined by paired two-tailed *t*-test for cytokine and viability data and by Mann–Whitney *U*-test with Bonferroni correction following Kruskal–Wallis *H*-test for microscopy data. Difference with $p < 0.05$ was considered significant.

Acknowledgments: We thank Bristol-Myers Squibb Company for providing dasatinib, Novartis Phama for providing imatinib and nilotinib, Masaki Yasukawa for providing HSV-1, Reiko Saito for providing influenza virus, Keiko Fukunaga (Kyoto University) for her excellent technical assistance, Takashi Uchiyama (Kyoto University) for his supervision, the physicians who provided blood samples from patients treated with the TKIs, and Shin-ichiro Fujii (RIKEN, Research Center for Allergy and Immunology, Japan) for reviewing the manuscript. This study was supported by research funding from Ministry of Education, Culture, Sports, Science, and Technology of Japan (17016034) and from Japan Science and Technology Agency, Core Research for Evolutional Science and Technology (CREST) (to N.K.).

Conflict of Interest: The authors declare no financial or commercial conflict of interest.

References

1 **Liu, Y.-J.**, IPC: professional type 1 interferon-producing cells and plasmacytoid dendritic cell precursors. *Annu. Rev. Immunol.* 2005. **23**: 275–306.

2 **Gilliet, M., Cao, W. and Liu, Y.-J.**, Plasmacytoid dendritic cells: sensing nucleic acids in viral infection and autoimmune diseases. *Nat. Rev. Immunol.* 2008. **8**: 594–606.

3 **Ganguly, D., Chamilos, G., Lande, R., Gregorio, J., Meller, S., Facchinetti, V., Homey, B. et al.**, Self-RNA-antimicrobial peptide complexes activate human dendritic cells through TLR7 and TLR8. *J. Exp. Med.* 2009. **206**: 1983–1994.

4 **Weisberg, E., Manley, P. W., Cowan-Jacob, S. W., Hochhaus, A. and Griffin, J. D.**, Second generation inhibitors of BCR-ABL for the treatment of imatinib-resistant chronic myeloid leukaemia. *Nat. Rev. Cancer* 2007. **7**: 345–356.

5 **Lombardo, L. J., Lee, F. Y., Chen, P., Norris, D., Barrish, J. C., Behnia, K., Castaneda, S. et al.**, Discovery of *N*-(2-chloro-6-methylphenyl)-2-(6-(4-(2-hydroxyethyl)- piperazin-1-yl)-2-methylpyrimidin-4-ylamino)thiazole-5-carboxamide (BMS-354825), a dual Src/Abl kinase inhibitor with potent antitumor activity in preclinical assays. *J. Med. Chem.* 2004. **47**: 6658–6661.

6 **Schade, A. E., Schieven, G. L., Townsend, R., Jankowska, A. M., Susulic, V., Zhang, R., Szpurka, H. and Maciejewski, J. P.**, Dasatinib, a small-molecule protein tyrosine kinase inhibitor, inhibits T-cell activation and proliferation. *Blood* 2008. **111**: 1366–1377.

7 **Fei, F., Yu, Y., Schmitt, A., Rojewski, M. T., Chen, B., Greiner, J., Götz, M. et al.**, Dasatinib exerts an immunosuppressive effect on CD8+ T cells specific for viral and leukemia antigens. *Exp. Hematol.* 2008. **36**: 1297–1308.

8 **Blake, S. J., Bruce Lyons, A., Fraser, C. K., Hayball, J. D. and Hughes, T. P.**, Dasatinib suppresses in vitro natural killer cell cytotoxicity. *Blood* 2008. **111**: 4415–4416.

9 **Salih, J., Hilpert, J., Placke, T., Grünebach, F., Steinle, A., Salih, H. R. and Krusch, M.**, The BCR/ABL-inhibitors imatinib, nilotinib and dasatinib differentially affect NK cell reactivity. *Int. J. Cancer* 2010. **127**: 2119–2128.

10 **Manley, P. W., Stiefl, N., Cowan-Jacob, S. W., Kaufman, S., Mestan, J., Wartmann, M., Wiesmann, M. et al.**, Structural resemblances and comparisons of the relative pharmacological properties of imatinib and nilotinib. *Bioorg. Med. Chem.* 2010. **18**: 6977–6986.

11 **Honda, K., Ohba, Y., Yanai, H., Negishi, H., Mizutani, T., Takaoka, A., Taya, C. and Taniguchi, T.**, Spatiotemporal regulation of MyD88-IRF-7 signalling for robust type-I interferon induction. *Nature* 2005. **434**: 1035–1040.

12 **Guiducci, C., Ott, G., Chan, J. H., Damon, E., Calacsan, C., Matray, T., Lee, K.-D. et al.**, Properties regulating the nature of the plasmacytoid dendritic cell response to Toll-like receptor 9 activation. *J. Exp. Med.* 2006. **203**: 1999–2008.

13 **Krieg, A. M.**, CpG motifs in bacterial DNA and their immune effects. *Annu. Rev. Immunol.* 2002. **20**: 709–760.

14 **Kerkmann, M., Costa, L. T., Richter, C., Rothenfusser, S., Battiany, J., Hornung, V., Johnson, J. et al.**, Spontaneous formation of nucleic acid-based nanoparticles is responsible for high interferon-{alpha} induction by CpG-A in plasmacytoid dendritic cells. *J. Biol. Chem.* 2005. **280**: 8086–8093.

15 **Lande, R., Gregorio, J., Facchinetti, V., Chatterjee, B., Wang, Y.-H., Homey, B., Cao, W. et al.**, Plasmacytoid dendritic cells sense self-DNA coupled with antimicrobial peptide. *Nature* 2007. **449**: 564–569.

16 **Krug, A., Rothenfusser, S., Hornung, V., Jahrsdorfer, B., Blackwell, S., Ballas, Z. K., Endres, S. et al.**, Identification of CpG oligonucleotide sequences with high induction of IFN-alpha/beta in plasmacytoid dendritic cells. *Eur. J. Immunol.* 2001. **31**: 2154–2163.

17 **Hanke, J. H., Gardner, J. P., Dow, R. L., Changelian, P. S., Brissette, W. H., Weringer, E. J., Pollok, B. A. and Connelly, P. A.**, Discovery of a novel, potent, and Src family-selective tyrosine kinase inhibitor. *J. Biol. Chem.* 1996. **271**: 695–701.

18 **Blake, R. A., Broome, M. A., Liu, X., Wu, J., Gishizky, M., Sun, L. and Courtneidge, S. A.**, SU6656, a selective Src family kinase inhibitor, used to probe growth factor signaling. *Mol. Cell. Biol.* 2000. **20**: 9018–9027.

19 **Latz, E., Schoenemeyer, A., Visintin, A., Fitzgerald, K. A., Monks, B. G., Knetter, C. F., Lien, E. et al.**, TLR9 signals after translocating from the ER to CpG DNA in the lysosome. *Nat. Immunol.* 2004. **5**: 190–198.

20 **Hirai, M., Kadowaki, N., Kitawaki, T., Fujita, H., Takaori-Kondo, A., Fukui, R., Miyake, K. et al.**, Bortezomib suppresses function and survival of plasmacytoid dendritic cells by targeting intracellular trafficking of Toll-like receptors and endoplasmic reticulum homeostasis. *Blood* 2011. **117**: 500–509.

21 **Manders, E. M. M., Verbeek, F. J. and Aten, J. A.**, Measurement of colocalization of objects in dual-color confocal images. *J. Microsc.* 1993. **169**: 375–382.

22 **Dunn, K. W., Kamocka, M. M. and McDonald, J. H.**, A practical guide to evaluating colocalization in biological microscopy. *Am. J. Physiol. Cell Physiol.* 2011. **300**: C723-C742.

23 **Costes, S. V., Daelemans, D., Cho, E. H., Dobbin, Z., Pavlakis, G. and Lockett, S.**, Automatic and quantitative measurement of protein-protein colocalization in live cells. *Biophys. J.* 2004. **86**: 3993–4003.

24 **Kaisho, T. and Tanaka, T.**, Turning NF-[kappa]B and IRFs on and off in DC. *Trends Immunol.* 2008. **29**: 329–336.

25 **Park, B., Brinkmann, M. M., Spooner, E., Lee, C. C., Kim, Y.-M. and Ploegh, H. L.**, Proteolytic cleavage in an endolysosomal compartment is required for activation of Toll-like receptor 9. *Nat. Immunol.* 2008. **9**: 1407–1414.

26 **Maeda, T., Murata, K., Fukushima, T., Sugahara, K., Tsuruda, K., Anami, M., Onimaru, Y. et al.**, A novel plasmacytoid dendritic cell line, CAL-1, established from a patient with blastic natural killer cell lymphoma. *Int. J. Hematol.* 2005. **81**: 148–154.

27 **Sanjuan, M. A., Rao, N., Lai, K.-T. A., Gu, Y., Sun, S., Fuchs, A., Fung-Leung, W.-P. et al.**, CpG-induced tyrosine phosphorylation occurs via a

TLR9-independent mechanism and is required for cytokine secretion. *J. Cell Biol.* 2006. **172**: 1057–1068.

28 **Liberali, P., Rämö, P. and Pelkmans, L.**, Protein kinases: starting a molecular systems view of endocytosis. *Annu. Rev. Cell Dev. Biol.* 2008. **24**: 501–523.

29 **Bantscheff, M., Eberhard, D., Abraham, Y., Bastuck, S., Boesche, M., Hobson, S., Mathieson, T. et al.**, Quantitative chemical proteomics reveals mechanisms of action of clinical ABL kinase inhibitors. *Nat. Biotechnol.* 2007. **25**: 1035–1044.

30 **Rix, U., Hantschel, O., Durnberger, G., Remsing Rix, L. L., Planyavsky, M., Fernbach, N. V., Kaupe, I. et al.**, Chemical proteomic profiles of the BCR-ABL inhibitors imatinib, nilotinib, and dasatinib reveal novel kinase and nonkinase targets. *Blood* 2007. **110**: 4055–4063.

31 **Karaman, M. W., Herrgard, S., Treiber, D. K., Gallant, P., Atteridge, C. E., Campbell, B. T., Chan, K. W. et al.**, A quantitative analysis of kinase inhibitor selectivity. *Nat. Biotechnol.* 2008. **26**: 127–132.

32 **Li, J., Rix, U., Fang, B., Bai, Y., Edwards, A., Colinge, J., Bennett, K. L. et al.**, A chemical and phosphoproteomic characterization of dasatinib action in lung cancer. *Nat. Chem. Biol.* 2010. **6**: 291–299.

33 **Sasai, M., Linehan, M. M. and Iwasaki, A.**, Bifurcation of Toll-Like receptor 9 signaling by adaptor protein 3. *Science* 2010. **329**: 1530–1534.

34 **Blasius, A. L., Arnold, C. N., Georgel, P., Rutschmann, S., Xia, Y., Lin, P., Ross, C. et al.**, Slc15a4, AP-3, and Hermansky-Pudlak syndrome proteins are required for Toll-like receptor signaling in plasmacytoid dendritic cells. *Proc. Natl. Acad. Sci. USA* 2010. **107**: 19973–19978.

35 **Lee, J., Tattoli, I., Wojtal, K. A., Vavricka, S. R., Philpott, D. J. and Girardin, S. E.**, pH-dependent internalization of muramyl peptides from early endosomes enables Nod1 and Nod2 signaling. *J. Biol. Chem.* 2009. **284**: 23818–23829.

36 **Di Pietro, S. M., Falcón-Pérez, J. M., Tenza, D., Setty, S. R. G., Marks, M. S., Raposo, G. and Dell'Angelica, E. C.**, BLOC-1 interacts with BLOC-2 and the AP-3 complex to facilitate protein trafficking on endosomes. *Mol. Biol. Cell* 2006. **17**: 4027–4038.

37 **Setty, S. R. G., Tenza, D., Truschel, S. T., Chou, E., Sviderskaya, E. V., Theos, A. C., Lamoreux, M. L. et al.**, BLOC-1 is required for cargo-specific sorting from vacuolar early endosomes toward lysosome-related organelles. *Mol. Biol. Cell* 2007. **18**: 768–780.

38 **Kawamura, K., Kadowaki, N., Kitawaki, T. and Uchiyama, T.**, Virus-stimulated plasmacytoid dendritic cells induce CD4 +cytotoxic regulatory T cells. *Blood* 2006. **107**: 1031–1038.

39 **Hartmann, G., Weeratna, R. D., Ballas, Z. K., Payette, P., Blackwell, S., Suparto, I., Rasmussen, W. L. et al.**, Delineation of a CpG phosphorothioate oligodeoxynucleotide for activating primate immune responses in vitro and in vivo. *J. Immunol.* 2000. **164**: 1617–1624.

Abbreviations: **ALL**: acute lymphoblastic leukemia · **AP**: adaptor protein · **BLOC**: biogenesis of lysosome-related organelles complex · **CML**: chronic myeloid leukemia · **DOTAP**: 1,2-dioleoyloxy-3-trimethylammonium-propane · **IRF**: IFN regulatory factor · **ODN**: oligodeoxynucleotide · **pDC**: plasmacytoid DC · **Ph**: Philadelphia · **SFK**: SRC family kinase · **TKI**: tyrosine kinase inhibitor

Full correspondence: Dr. Norimitsu Kadowaki, Department of Hematology and Oncology, Graduate School of Medicine, Kyoto University, 54 Shogoin Kawara-cho, Sakyo-ku, Kyoto 606-8507, Japan
Fax: +81-75-751-4963
e-mail: kadowaki@kuhp.kyoto-u.ac.jp

Received: 23/5/2012
Revised: 21/9/2012
Accepted: 24/10/2012
Accepted article online: 30/10/2012

Leukemia (2012), 1–4

www.nature.com/leu

LETTER TO THE EDITOR

Direct binding of Grb2 has an important role in the development of myeloproliferative disease induced by ETV6/FLT3

Leukemia advance online publication, 14 December 2012; doi:10.1038/leu.2012.333

FMS-like tyrosine kinase 3 (*FLT3*) is one of the most frequently mutated genes in hematological malignancies.[1] The most common mutations of *FLT3* are internal tandem duplications (ITDs) within the juxtamembrane domain, which occur in 20% to 30% of patients with acute myeloid leukemia (AML).[2,3] Although FLT3 is a potential therapeutic target in AML, recent studies involving FLT3 inhibitors as single agents in patients with AML showed limited clinical responses.[4] FLT3 has been reported to fuse to ETV6 (TEL) in a few cases of myeloid/lymphoid neoplasms with eosinophilia (MLN-eo) carrying a translocation t(12;13)(p13;q12).[5,6] Although it has been shown that ETV6/FLT3 acts as a constitutively active tyrosine kinase, the molecular mechanisms underlying ETV6/FLT3-mediated leukemogenesis remain incompletely understood.[7–9]

We identified a novel *ETV6/FLT3* variant fusion transcript (E/F-1) in a MLN-eo patient (Supplementary Figures S1A and B) and investigated the transforming properties of ETV6/FLT3 *in vivo* using a murine bone marrow transplant (BMT) model.[10,11] E/F-1-transduced recipients developed an aggressive polyclonal myeloproliferative disease (MPD) in 100% of recipient mice with a latency of 3-4 weeks, as evidenced by marked leukocytosis, splenomegaly and massive expansion of myeloid cells in peripheral blood, spleen and bone marrow (Figures 1A–C). In this mice model, eosinophilia was not observed. Flow cytometric analysis of the peripheral blood from E/F-1 mice showed a large population of $EGFP^+/Mac\text{-}1^+/Gr\text{-}1^+$ cells. In primary E/F-1 mice, serial passage was performed by transferring a 1:1 mixture of spleen and bone marrow cells to sublethally irradiated recipient mice. This resulted in hematopoietic malignancies in most of the recipient mice receiving five different primary tumors. For three of the primary tumors, it was possible to transmit the MPD for at least one round. In all cases of serial passage, the MPD transformed into aggressive T-lymphoblastic lymphoma (T-LBL) with a latency of 4–17 weeks (Figure 1E, Supplementary Figure S2B). Most lymphoma occurred in the thymus or abdominal lymph nodes, and some of the secondary recipient mice displayed leukocytosis, generalized lymphadenopathy or hepatosplenomegaly. Histopathological examination revealed that the architecture of the lymph nodes and the thymus was completely effaced and that they contained a uniform population of lymphoblasts. The liver showed prominent periportal, lobular and sinusoidal infiltration by lymphoma cells (Figure 1D). Flow cytometric analysis of spleen cells revealed that the lymphomas typically showed an immature T-cell immunophenotype characterized by expression of both CD4 and CD8 (Supplementary Figure S2A). Affected tissues from secondary diseased mice contained proviral integrations identical to those in the primary MPD mouse (Figure 1F). ETV6/FLT3-induced T-LBL was transplantable, with all tertiary transplant recipients rapidly succumbing to T-LBL at 4–7 weeks after transfer arising from common clones identified in the secondary mice (Supplementary Figure S2C).

Previous studies have shown that FLT3-ITDs induce a lethal MPD in mice and that tyrosine residues 589 and 591 in the juxtamembrane domain of FLT3 are critical for STAT5 phosphorylation and generation of the MPD phenotype.[10] We also demonstrated the corresponding results for FLT3-ITD in our murine BMT experiment (Supplementary Figures S3A and B). On the other hand, mice that received the double tyrosine-to-phenylalanine mutant of E/F-1 at sites 589 and 591 (Y589/591F) in the juxtamembrane domain of FLT3 developed a similar MPD (Supplementary Table S1). There was no significant difference in survival between recipients of E/F-1 vs Y589/591F, with both mice groups succumbing to a fatal MPD within a median survival time of 18 and 19.5 days, respectively ($P = 0.284$; Figure 1C). The Y589/591F mutation did not abrogate STAT5, Erk1/2 and Akt activation in Ba/F3 cells transformed by E/F-1 (Supplementary Figure S4), which is consistent with the previous studies using a deletion mutant of the FLT3 juxtamembrane domain in ETV6/FLT3.[9]

Growth factor receptor-binding protein 2 (Grb2) is an adaptor protein known to bind several receptor tyrosine kinases. Grb2 binds the scaffolding protein Grb2-associated binder 2 (Gab2) and contributes to survival signaling in ligand-activated wild-type FLT3.[12] A recent study has shown that tyrosines 768, 955 and 969 of FLT3 are the direct Grb2-binding sites of importance for FLT3-ITD-mediated proliferation and survival of hematopoietic cells *in vitro* as a result of STAT5 activation via Gab2.[13] However, there have been no reports regarding the *in vivo* effects of direct Grb2 binding by oncogenic FLT3 in leukemogenesis. Thus, we investigated the role of Grb2 binding in ETV6/FLT3-mediated leukemogenesis. Inspection of the ETV6 portion of the fusion protein revealed only two candidate tyrosines for direct binding of Grb2 at positions 314 and 354. To test whether Grb2 binds directly to ETV6/FLT3, we made a series of Grb2-binding mutants of ETV6/FLT3 (Figure 2a). The Y314/354F double point mutant (2F) and the Y768/955/969F triple mutant (3F-1) of E/F-1 showed a reduced ability to bind Grb2 as compared with the E/F-1. Furthermore, when we mutated tyrosines 314 or 354 to phenylalanine in the context of the Y768/955/969F triple mutant, the association of ETV6/FLT3 with Grb2 was significantly reduced as compared with the Y768/955/969F triple mutant. Finally, when we mutated all five specific tyrosines (Y314/354/768/955/969) to phenylalanine, we observed that ETV6/FLT3 was no longer able to bind Grb2 (Figure 2b). Simultaneous mutation of these five tyrosine residues resulted in an absence of Gab2 phosphorylation, and impaired activation of STAT5, Erk1/2 and Akt in Ba/F3 cells (Figure 2c). ETV6/FLT3 variant E/F-2, which lacked the Grb2-binding sites of ETV6, was unable to bind to Grb2 when all three Grb2-binding sites of FLT3 were mutated (Figure 2b). This Y768/955/969F triple mutant of E/F-2 (3F-2) was also unable to phosphorylate Gab2 and showed weaker activation of STAT5, Erk1/2 and Akt as compared with E/F-2 in Ba/F3 cells (Figure 2c). Both E/F-1 and E/F-2 transformed bone marrow cells to be capable of cytokine-independent growth in methylcellulose medium. Transformation was significantly decreased in the 5F and 3F-2 mutants, which

Accepted article preview online 20 November 2012